Chemical Science

ROYAL SOCIETY OF CHEMISTRY

REVIEW

View Article Online
View Journal | View Issue

Cite this: *Chem. Sci.*, 2024, **15**, 4292

Customizing catalyst surface/interface structures for electrochemical CO_2 reduction

Xin Tan,†[a] Haojie Zhu,†[a] Chang He,[a] Zewen Zhuang,[c] Kaian Sun,[c] Chao Zhang*[b] and Chen Chen*[a]

Received 29th December 2023
Accepted 26th February 2024

DOI: 10.1039/d3sc06990g

rsc.li/chemical-science

Electrochemical CO_2 reduction reaction (CO_2RR) provides a promising route to converting CO_2 into value-added chemicals and to neutralizing the greenhouse gas emission. For the industrial application of CO_2RR, high-performance electrocatalysts featuring high activities and selectivities are essential. It has been demonstrated that customizing the catalyst surface/interface structures allows for high-precision control over the microenvironment for catalysis as well as the adsorption/desorption behaviors of key reaction intermediates in CO_2RR, thereby elevating the activity, selectivity and stability of the electrocatalysts. In this paper, we review the progress in customizing the surface/interface structures for CO_2RR electrocatalysts (including atomic-site catalysts, metal catalysts, and metal/oxide catalysts). From the perspectives of coordination engineering, atomic interface design, surface modification, and hetero-interface construction, we delineate the resulting specific alterations in surface/interface structures, and their effect on the CO_2RR process. At the end of this review, we present a brief discussion and outlook on the current challenges and future directions for achieving high-efficiency CO_2RR *via* surface/interface engineering.

1. Introduction

In recent years, the global annual CO_2 emission due to fossil fuel consumption has been on an alerting high level. Approximately half of the emission could be neutralized by land and ocean *via* the natural carbon cycle, and the other half accumulates in the Earth's atmosphere, resulting in pressing issues relating to environment and sustainability.[1–3] According

Xin Tan

Xin Tan received his BS degree from the School of Materials Science and Engineering at Wuhan University of Technology in 2019. He is now a PhD candidate in Prof. Chen Chen's group in the Department of Chemistry, Tsinghua University. His research interests are focused on developing new catalysts for electrochemical CO_2 reduction.

Chen Chen

Chen Chen is a professor at Department of Chemistry in Tsinghua University. He received his B.S. in 2006 from Beijing Institute of Technology, and PhD in 2011 from Tsinghua University. He worked as a postdoctoral researcher at Lawrence Berkeley National Laboratory and UC Berkeley from 2011 to 2014, and joined the faculty of Tsinghua University in 2015. His research interest is focused on inorganic materials, catalysis, renewable and sustainable energy. Prof. Chen has published over 100 scientific papers with more than 20 000 citations and an H-index of over 60. He was designated a Highly Cited Researcher (2021–2023) by Clarivate.

---

[a] *Engineering Research Center of Advanced Rare Earth Materials, Department of Chemistry, Tsinghua University, Beijing 100084, China. E-mail: cchen@mail.tsinghua.edu.cn*

[b] *MOE International Joint Laboratory of Materials Microstructure, Institute for New Energy Materials and Low-Carbon Technologies, School of Materials Science and Engineering, Tianjin University of Technology, Tianjin 300384, China. E-mail: czhang@email.tjut.edu.cn*

[c] *College of Materials Science and Engineering, Fuzhou University, Fuzhou 350108, China*

† Xin Tan and Haojie Zhu contributed equally to this work.

to statistics from the Energy & Climate Intelligence Unit, more than 130 countries and regions have proclaimed the goal of "zero carbon" or "carbon neutrality", and thus effective measures have to be taken to lower the atmospheric CO_2 concentration.[4,5] To this end, CO_2 conversion and utilization has been proposed as a potential solution to carbon neutrality. In particular, CO_2 could be electrochemically reduced into fuels and commodity chemicals; when integrated with renewable electricity (such as solar and wind power), this electrochemical route is expected to close the carbon cycle.[6] However, CO_2 is notorious for its chemical inertness, the activation of CO_2 molecules generally has to overcome a high energy barrier, and the practical implementation of electrochemical CO_2 reduction reaction (CO_2RR) faces a number of challenging issues, such as high overpotentials, competing side reactions (most notably, hydrogen evolution reaction, HER), and diverse reduction products.[7–9] As a result, one of the major topics in CO_2RR is to design and construct catalytic materials with optimized activities and selectivities.

The customization of catalyst surface/interface refers to the approach that resorts to design and modulate the structures and properties of catalyst surface/interface, so as to optimize the catalytic performance.[10–12] In the past few decades, with the emergence of advanced methodologies in both experimental characterization and theoretical simulation, the research focus of catalysis has shifted from observing and documenting the macroscopic catalytic phenomena to monitoring and deciphering catalytic processes on the atomic/molecular level.[2,13–15] The idea of structure/mechanism-oriented catalyst design has thus emerged, which offers immense opportunities for developing high-performance CO_2RR catalysts. Some catalytic systems with specific structures and functions can now be constructed *via* rational design; with the surface/interface reaction processes ideally customized, catalysts with superior activities, selectivities and stabilities can be obtained eventually. Such customization strategies include manipulating the crystallographic structures of the catalysts so as to expose specific atomic sites,[16,17] altering the coordination configurations so as to optimize the electronic structures of active centers (in particular, the coordination number and configuration of metal active centers),[18,19] modifying the surfaces/interfaces so as to regulate the microenvironment,[13,20] and constructing hetero-interfaces so as to promote the adsorption and activation of substrate molecules and intermediate species.[21,22] In addition, only by looking deep into the surface/interface structures of catalysts can we establish the structure–performance relationship for CO_2RR catalysis, which is of fundamental importance for developing more advanced electrocatalysts.[2,23]

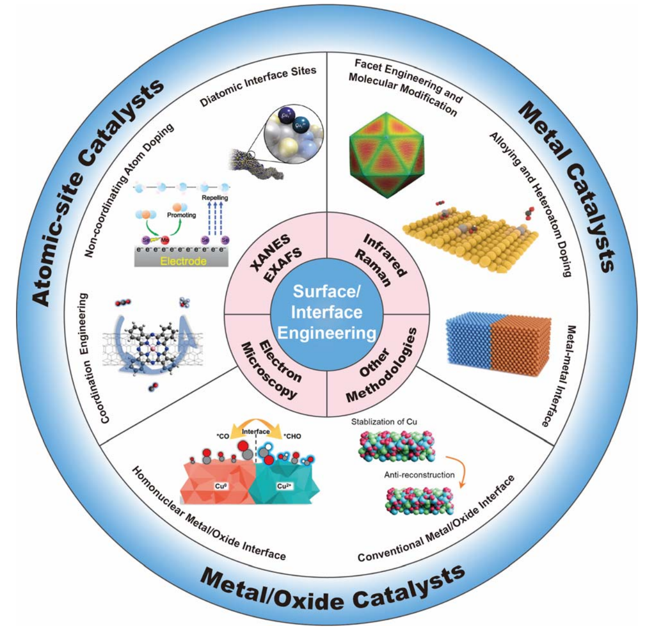

Fig. 1 Overview of the surface/interface engineering for CO_2RR catalysts.

In this review, we start with an overview of the advanced methodologies for probing the structures of catalyst surfaces/interfaces (including synchrotron-radiation-based X-ray absorption spectroscopy, atomic-resolution electron microscopy, and infrared spectroscopy), which could offer more in-depth insights into catalytic structures at the atomic level. Subsequently, we present a systematic overview on the recent progress in customizing the surfaces/interfaces of CO_2RR electrocatalysts, including atomic-site catalysts (*e.g.*, single-atomic-site catalysts, diatomic-site catalysts), metal catalysts, and metal/oxide catalysts. From the perspectives of coordination engineering, atomic interface design, surface modification, and hetero-interface construction, we delineate the resulting specific alterations in surface/interface structures, and their effect on the CO_2RR process, including (but not limited to) microenvironment modulation, enrichment of substrate molecules, adsorption/desorption of intermediate species. At the end of this review, we give a discussion on the challenges currently faced in the field of surface/interface engineering of CO_2RR electrocatalysts, and present an outlook on the possible future directions in this field (Fig. 1).

2. Advanced methodologies for probing the structures of catalyst surfaces/interfaces

In the realm of surface/interface engineering, a profound exploration for advanced structural characterization methodologies is imperative. By employing advanced techniques, one can gain a more comprehensive and in-depth understanding of the microscopic structural features of catalyst surfaces and interfaces. In this section, we will discuss advanced characterization techniques and corresponding *in situ* and operando techniques under CO_2RR test conditions, aiming to unveil the unique structural characteristics of catalyst surfaces/interfaces and to lay the groundwork for achieving efficient CO_2RR.

2.1 X-ray absorption spectroscopy

X-ray absorption spectroscopy (XAS) has become one of the most popular methodologies for probing information regarding the structures of catalyst surfaces/interfaces.[24] This characterization technique has achieved notable success in probing the surface/interface site structure of single-atomic catalysts. For instance, one can determine the local coordination configuration of synthesized catalysts, such as the FeN_4 structure or FeN_4O structure, through fitting the spectra.[25,26] It is important to note that distinguishing ligand atoms (such as C, N and O) using XAS is quite challenging, and often requires complementary techniques such as X-ray emission spectroscopy (XES) for a more comprehensive assessment.[25] At the solid–liquid interface in electrocatalysis, the dynamically evolving catalyst surface, where reactants, intermediates, and product species coexist, is often referred to as having disordered features rather than ordered crystalline properties.[27] In this regard, operando XAS is one of the characterization techniques capable of revealing the real dynamic configuration of the structures of catalyst surface/interface. Timoshenko *et al.* utilized time-resolved operando XAS to investigate the impact of the duration of pulse oxidation potential and reduction potential (Δt_a and Δt_c) on the surface oxidation state of copper catalysts (Fig. 2(a)).[28] The results indicate that both surface defects and oxidation states can enhance ethanol production. On the basis of these results, a coordinated optimization of Δt_a and Δt_c was employed to balance the oxidation state and morphology, leading to the identification of a region that significantly promotes ethanol generation (Fig. 2(b)).

2.2 Atomic-resolution electron microscopy

Advancements in materials science and catalysis research demand an in-depth understanding of catalyst surfaces and interfaces at the atomic level. Electron microscopies have evolved significantly, enabling scientists to probe catalyst surfaces with unparalleled precision, uncovering details crucial for optimizing catalytic performance. The work of Chung *et al.* serves as a groundbreaking example; they pioneered the use of aberration-corrected high-angle annular dark-field scanning transmission electron microscopy (AC-HAADF-STEM) combined with electron energy loss spectroscopy (EELS) to directly observe the configuration of Fe–N_4 for the first time.[29] This study provides crucial guidance for subsequent structural analyses of M–N–C catalysts at the atomic level and their exploration in various catalytic applications. Additionally, our research group identified "true" dual-atomic sites through *in situ* rotation manipulation using AC-HAADF-STEM (Fig. 2(c)).[30] Operando electrochemical liquid-cell scanning transmission electron microscopy (EC-STEM) enables imaging with high spatial resolution at the nanometer scale within a liquid environment under electrochemical reaction conditions. This technique has been employed to track the changes in the surface/interface structure of nanocatalysts under CO_2RR conditions. Employing this approach, Yang *et al.* used 7–18 nm copper nanoparticles as model catalysts to comprehensively reveal the evolution of copper nanocatalysts during the reaction process (Fig. 2(d–h)).[23] On the basis of EC-STEM results, the team further developed a four-dimensional scanning transmission electron microscopy (4D-STEM) structural characterization technique to unveil the evolution processes of copper catalysts.

2.3 Other methodologies

Raman and infrared spectroscopies could serve as powerful tools for monitoring surface-adsorbed molecules and intermediate species involved in electron/proton transfer and bond formation under CO_2RR conditions.[31,32] Moreover, they also demonstrate great potential in probing the structures of catalyst surfaces/interfaces. For instance, *in situ* diffuse reflectance infrared Fourier transform spectroscopy (DRIFTS) of CO adsorption has been conducted to determine the distribution state of Rh in CuRh alloy, where Rh single atoms and Rh clusters exhibited distinctly different CO adsorption peak shapes.[33] To investigate the structural evolution of the Bi_2O_3 catalyst during the CO_2RR, Broekmann *et al.* utilized Raman spectroscopy to identify Bi_{metal}, Bi_2O_3, and $Bi_2O_2CO_3$ phases and proposed two pathways for formate production based on experimental results: the "sub-carbonate" pathway at low overpotentials and the $Bi_{metal\text{–}O}$ pathway at high overpotentials (Fig. 2(i and j)).[34] Additionally, the team employed X-ray diffraction computed tomography (XRD-CT) to analyze the spatial distribution of the chemical composition after the reaction with a relatively high spatial resolution (40 μm), confirming that the distribution of $Bi_2O_2CO_3$ and Bi_{metal} phases is rather homogeneous as a function of the catalyst layer depth (Fig. 2(k)).[35]

The combination of experimental and theoretical approaches offers a novel avenue to investigating the structures of catalyst surfaces/interfaces. Klinkova *et al.* utilized *ex situ* high-resolution scanning electron microscopy (SEM) and electrochemical surface analysis through underpotential deposition (UPD) to explore the structural behavior of well-defined gold and palladium core cages and branched nanoparticles during CO_2RR processes.[36] On the basis of experimental trends and the integration of density functional theory (DFT) and finite element method (FEM) calculations, the team proposed a mechanistic description of their structural dynamics (Fig. 2(l)). Specifically, the team unveiled the interaction of electrochemical effects (atomic migration facilitated by adsorption reaction intermediates) and electronic effects (electron migration). Both of these effects were identified as driving forces for structural transformations in the materials. The theoretical foundation established in this work serves as a predictive method for assessing the electrochemical surface/interface structural behaviors of novel materials. In summary, these pioneering methodologies offer robust support for future catalyst design and optimization, enabling us to precisely control the structures of catalyst surfaces/interfaces and promote the development of CO_2RR.[37,38]

3. Surface/interface engineering for atomic-site catalysts

The advancements in both preparation methods and characterization techniques have sparked significant interest in

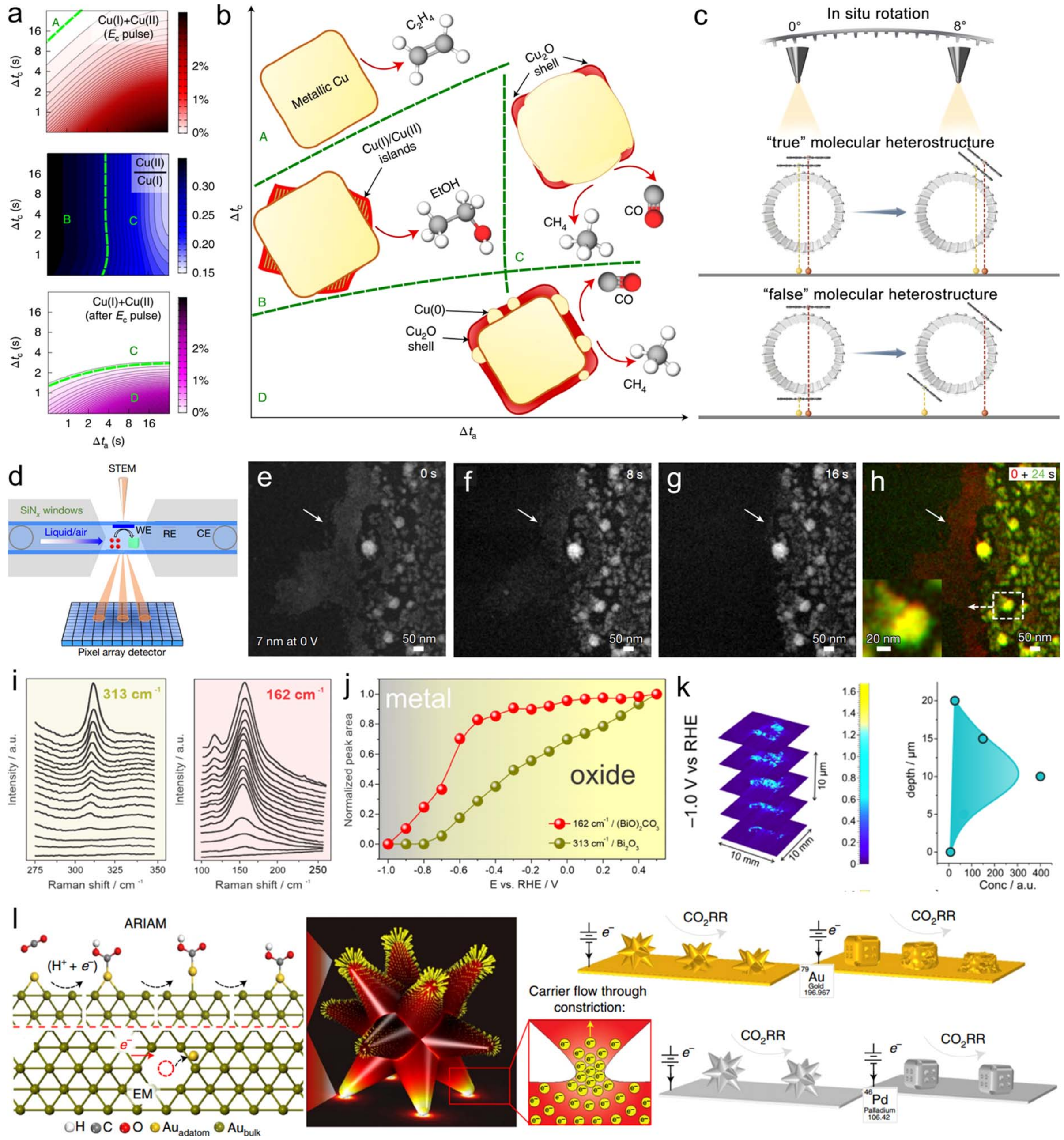

Fig. 2 (a) The results obtained from the analysis of XAS data for copper catalyst during pulsed CO_2RR with $E_{anode} = 0.6$ V, showing the average concentration of the oxide species present during the cathodic pulse. (b) Evolution of the copper catalyst structure and composition during a cathodic pulse extracted from XAS and XRD data. Reproduced with permission from ref. 28. Copyright 2022, Springer Nature. (c) *In situ* rotation in AC-HAADF-STEM characterization to differentiate the "true" and "false" dual-atomic sites. Reproduced with permission from ref. 30. Copyright 2023, American Chemical Society. (d) Schematic of operando EC-STEM and 4D-STEM. Morphological evolution of 7 nm NPs at 0 V *vs.* RHE at 0 (e), 8 (f), 16 (g) and 24 s (h). Reproduced with permission from ref. 23. Copyright 2023, Springer Nature. (i) Potential-dependent changes of the Raman peak at 313 cm^{-1} and 162 cm^{-1} used as the fingerprint for the presence of Bi_2O_3 and $Bi_2O_2CO_3$, respectively. (j) Potential-dependent integrated intensities of the Raman peaks shown in (i). Reproduced with permission from ref. 34. Copyright 2021, American Chemical Society. (k) XRD-CT scans of the catalyst layer after CO_2RR (1 h) at −1 V *vs.* RHE. Reproduced with permission from ref. 35. Copyright 2022, American Chemical Society. (l) Illustration of the factors driving atomic migration in electrocatalysts. Reproduced with permission from ref. 36. Copyright 2021, Springer Nature.

atomic-site catalysts. For one thing, atomic-site catalysts theoretically offer the highest atomic utilization efficiency, aligning with the principles of green chemistry. For another thing, they not only possess distinctive structural features and high activity similar to homogeneous catalysts but also exhibit ease of separation from reaction system. By precisely manipulating the coordination environment of atomic sites, researchers can alter the adsorption/desorption processes of key intermediates in the

CO_2RR process, thus modulating the activity and selectivity of the catalyst.[6] Moreover, the electrocatalytic process of CO_2RR involves the participation of multiple molecules such as water and carbon dioxide, making the design of synergistic catalytic systems or reaction microenvironments crucial in addition to directly modulating the intrinsic activity of ASCs.[39,40] This section summarizes the rational design strategies for ASCs interfaces focused on coordination engineering, non-coordinating atom doping, and construction of diatomic interface sites.

3.1 Coordination engineering

The two most direct influencing factors of the coordination environment are the identity of the coordinating atoms and the coordination number. Therefore, this section primarily emphasizes two coordination engineering strategies: coordinating atom engineering and coordination number engineering.

3.1.1 Coordinating atom engineering. Modulating the atoms in the first coordination shell around the metal active site enables the direct alteration of the oxidation state and electronic structure of the metal centers, thereby exerting a significant influence on the catalytic performance of the catalyst. Fe SAC with FeN_4 sites has been reported for its great potential to replace conventional precious-metal-based catalysts in CO_2RR, as it could give a lower overpotential for the CO_2-to-CO conversion.[41] However, suffering from serious competing hydrogen evolution reaction (HER), Fe–N–C catalysts could effectively produce CO only in a narrow potential range, the ultimate cause behind which is the inadequate adsorption/desorption energy of key intermediates. To solve this problem, Zhao *et al.* built novel $Fe_1N_2O_2$ sites on N-doped carbon derived from nitrogen source assisted pyrolysis of an oxygen-abundant MOF precursor. By replacing two coordinating N atoms with two O atoms, the team successfully optimized the kinetic activation processes of the CO_2RR at the Fe_1 sites. Theoretical calculations revealed that, compared with N, the coordinating O atoms could significantly lower the free energy change for the steps of both *COOH formation and CO desorption, and as such, the $Fe_1N_2O_2$/NC catalyst exhibited a broad potential range from −0.4 to −0.8 V while maintaining a high selectivity of 95% for CO.[39]

Another notable example for coordinating atom engineering is the Ga_1 site in CO_2RR. Ga nanomaterials are capable of thermally reducing CO_2 to generate solid carbon, whereas Ga metal and Ga_2O_3 exhibit poor CO_2RR performance.[42] Zhang *et al.* reported the development of a Ga-N_3S-PC catalyst by downsizing the active center of the main group element gallium to the atomic level. By incorporating S atoms in the first coordination shell and P atoms in the external coordination shell, the electronic environment of Ga_1 sites is significantly altered, resulting in an increase in the Gibbs free energy barriers for HER and a decrease in those for CO_2RR. Consequently, the Ga-N_3S-PC catalyst demonstrates a FE_{CO} of approximately 92% at −0.3 V *vs.* RHE. Theoretical simulations revealed the presence of an adaptive dynamic transition of Ga, during which the continual reconfiguration of Ga–S and Ga–P bonds can optimize the adsorption energy of the *COOH intermediate and regenerate the active sites in a timely manner, leading to significantly enhanced CO_2RR selectivity and stability compared with Ga–N_4 (Fig. 3(a)).[43] Therefore, manipulating the coordinating atoms (even in the external coordination shell) can lead to better mimicking of molecular catalysts. Similarly, in addition to the two-electron reduction product CO, by altering the adsorption mode and strength of intermediates, Zn and Co atomic sites have the potential to produce a more diverse array of products in CO_2RR, including methanol and methane.[40,44]

3.1.2 Coordination number engineering. In addition to the coordinating atoms, the coordination number of metal centers stands out as a crucial factor affecting their electronic structures. The incorporation of axial coordination, leading to the formation of a penta-coordinated structure, plays a pivotal role in regulating spin states and electronic properties, such as the d-band centers of the metal sites.[45] In this context, Chen *et al.* successfully synthesized a Fe_1N_4–O_1 site with axial O coordination using a rapid pyrolysis and controllable activation strategy.[26] XAS and AC-HAADF-STEM confirmed this unique coordination structure. The study demonstrated that the axial O coordination could contribute to the enhancement of electronic localization at the active sites, thereby increasing the energy barrier for HER and promoting CO desorption. By introducing the axial O coordination, the catalyst exhibited nearly 100% CO selectivity over a wide voltage range (Fig. 3(b)). Similarly, Pan *et al.* reported that a Co–N_5 structure displays enhanced CO_2RR performance, which is attributed to the lower *COOH formation energy barrier for Co–N_5 compared with Co–N_4.[19]

In addition to CO selectivity, coordination number engineering could also enhance current density and catalyst durability. Huang *et al.* developed a single-atom nanozyme (Ni–N_5–C) with a square-pyramidal Ni–N_5 site.[46] Because of the axial N coordination, the energy levels of the d_{z^2} and $d_{xz/yz}$ orbitals of the Ni–N_5 site were increased and decreased, respectively, compared with that for the Ni–N_4 site. This results in a decrease in the *CO_2-to-*COOH activation barrier and enhanced CO desorption, thereby boosting the kinetic activation process and catalytic performance. In catalytic tests for CO_2 reduction, the Ni–N_5–C catalyst demonstrated an impressive FE_{CO} of 99.6%, with a turnover frequency of 69.7 s^{-1}, under an ultra-high current density of 1.23 A cm^{-2}. Furthermore, the catalyst displayed a remarkable stability over a 100 hour period, surpassing numerous other reported single-atom catalysts. Moreover, for main group elements, the axial coordination has proved to be a crucial factor in imparting catalytic activity. Deng *et al.* developed a series of well-defined Sn single-atom catalysts as model systems to investigate their electrochemical reactivity for CO_2RR.[18] Through a combination of DFT calculations and *in situ* characterization experiments, the team demonstrated that the key site for CO_2 reduction into formic acid involves an axial O coordination in the O–Sn–N_4 structure. This site facilitates the CO_2-to-HCOOH conversion by promoting the formation of surface-bound bidentate tin carbonate species (Fig. 3(c)). Alto sum up, axial coordination engineering provides a versatile approach to regulating the coordination environment of single-

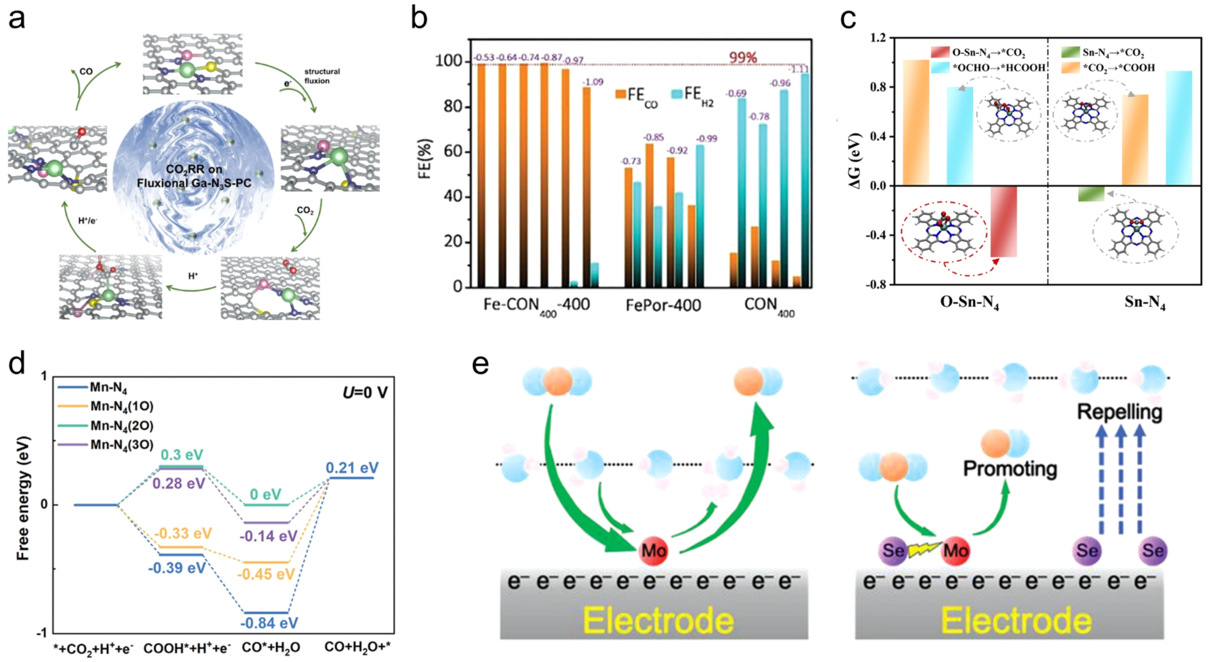

Fig. 3 (a) Schematic diagram of the catalytic CO_2RR process on fluxional GaN_3S-PC catalyst. Reproduced with permission from ref. 43. Copyright 2023, Wiley-VCH. (b) FE_{CO} and FE_{H_2} of Fe-CON_{400}-400, FePor-400 and CON_{400} at different potentials. Reproduced with permission from ref. 26. Copyright 2021, The Royal Society of Chemistry. (c) Calculated Δ*G* for CO_2RR over O–Sn–N_4 and Sn–N_4 sites. Reproduced with permission from ref. 18. Copyright 2023, American Chemical Society. (d) Calculated Δ*G* for CO_2RR to CO on the Mn–N_4, Mn–N_4(O), Mn–N_4(2O), and Mn–N_4(3O) surfaces. Reproduced with permission from ref. 53. Copyright 2023, Wiley-VCH. (e) Schematic diagram of the reaction mechanism of CO_2RR on the MoSA–SeSA catalyst. Reproduced with permission from ref. 55. Copyright 2022, Wiley-VCH.

atom sites, offering insights that are poised to deepen our understanding of the catalytic pathways and mechanisms involved in CO_2RR.

In addition to coordinating atom engineering and coordination number engineering, the dynamic structural evolution of atomic-site catalysts under reaction conditions significantly influences their catalytic performance.[47] In particular, the phenomena of reversible transformation between isolated atoms, metal clusters, and metal nanoparticles are of great importance for understanding the catalyst surface/interface structures and the true active centers for CO_2RR. For instance, Hsu *et al.* utilized *in situ* electrochemical transmission electron microscopy (EC-TEM) to image the dynamic changes of atomic-site catalysts during CO_2RR for the first time.[48] This structural reconfiguration can generate low-coordinated Cu SACs, which exhibit significantly high selectivity and activity to CO production. Similarly, NiN_2 sites originated from nitrogen vacancy induced coordinative reconstruction also demonstrate enhanced CO_2RR catalytic activity.[49] Furthermore, Cu SACs with CuN_4 sites were found to efficiently convert CO_2 to ethanol, with a faradaic yield as high as 55%.[50] Operando XAS experiments indicate that under reaction conditions, the reconstruction of CuN_4 sites forms metallic Cu nanoparticles, which are the truly catalytically active species. Interestingly, such reconstruction behavior is reversible, rendering the material a stable catalyst. With the advancement of characterization techniques, the reconstruction phenomenon of Cu SACs has garnered widespread attention in recent years. Other factors such as the applied potentials and the affinity between isolated Cu sites and coordinating atoms are considered to be closely related to this evolution process,[51] offering the possibility of further understanding and optimizing the surface/interface structure of atomic-site catalysts.

3.2 Non-coordinating atom doping

In addition to direct coordination interactions with active metal atoms, the presence of non-coordinating atoms doped within the catalyst support could also play a significant role in regulating the performance of atomic-site catalysts. On one hand, non-coordinating dopant atoms can alter the electronic structures of active sites through long-range interactions, thereby regulating the adsorption/desorption processes of intermediates and in turn modulating the catalytic performance.[52,53] On the other hand, doping of foreign atoms within the support is crucial in altering the microenvironment of the catalyst surface.[25] In the case of CO_2RR, where HER acts as a notable competing reaction, the presence of interfacial water greatly would impact the activity and selectivity of the catalyst. Thus, non-coordinating atom doping provides an additional means of tuning the atomic sites, particularly at the catalyst surface microenvironment, including the interfacial water.

3.2.1 Electronic structure optimization. As an electron donor when incorporated into carbon supports, P atoms can alter the electronic structures of atomic sites through its 3p lone-pair electrons, thus regulating their electrochemical activities. In this regard, Sun *et al.* employed a "host–guest" strategy and electrostatic adsorption to introduce single P atoms and single Fe atoms into the nitrogen-doped carbon materials.[52] XPS reveals that the synthesized Fe-SAC/NPC retains the Fe–N_4 coordination mode, indicating that P atoms existed in the form of P–C bonds in the support, rather than bonding with Fe. Additionally, DFT calculations demonstrate that P atoms in the outer coordination shells, particularly in the third coordination shell, could enhance the electron density at the Fe_1 sites, thus facilitating the formation of the key intermediate *COOH and lowering the overpotential for CO_2RR. The doping of P atoms into the support enabled the Fe-SAC/NPC catalyst to achieve a 97% CO selectivity at an overpotential of 320 mV, with a Tafel slope as low as 59 mV dec^{-1}.

Following a similar approach, Wang *et al.* investigated the relationship between the catalytic activity and the local structures of Mn–N–C catalysts through DFT calculations.[53] The results revealed that the introduction of different amounts of oxygen atoms in the second coordination shell can effectively improve the CO desorption from the Mn–N_4 surface to varying degrees (Fig. 3(d)). On the basis of this finding, they successfully introduced epoxy groups near the Mn–N_4 sites through a versatile nanoemulsion assembly approach. The resulting catalyst exhibited an enhanced electrocatalytic performance, achieving a high FE_{CO} of 94.5% at a low overpotential of 0.44 V in aqueous environments. Further calculations indicated that the adjacent epoxy groups to the Mn–N_4 sites could lower the d-band center of the Mn site, thus weakening the binding strength with CO. This decrease in the energy barrier for CO desorption significantly promoted the CO_2RR kinetics. It is worth mentioning that through the doping of non-coordinating oxygen atoms, this catalyst also demonstrated high performance in aprotic Li–CO_2 batteries, exhibiting an improved reversibility and a long cycling life.

3.2.2 Microenvironment optimization. The presence of pyridinic and pyrrolic nitrogen atoms in the Fe–N–C catalysts significantly hampers its selectivity for CO because of their strong affinity to proton. Therefore, it is necessary to tune the electrified interfaces of catalysts by regulating these non-coordinating atoms. Liu *et al.* employed a 5% H_2 inert gas atmosphere during high-temperature pyrolysis to convert the undesired pyridinic and pyrrolic N atoms in the Fe–N–C catalyst into graphitic N.[25] *In situ* attenuated total reflection surface-enhanced infrared absorption spectroscopy (ATR-SEIRAS) and DFT computations demonstrate that the graphitic N could not only suppress HER by eliminating “protophilic sites”, but also interact with FeN_4 to achieve synergistic adsorption of H_2O and CO_2, thereby facilitating the conversion of CO_2 into the *COOH intermediate. Through the manipulation of non-coordinating N dopants in the Fe–N–C catalyst, this study reports an FE_{CO} above 90% across a wide potential range from −0.3 to −0.8 V *vs.* RHE.

In addition to directly manipulating the non-coordinating atoms in the support, doping the support with a second element is another approach to regulating the interfacial water of single-atomic-site catalysts. Inspired by the Mo-dependent formate dehydrogenase found in nature, researchers infer that Mo single-atomic sites hold great potential in the field of CO_2RR.[54] Theoretical simulations have also confirmed the strong interaction between Mo atoms and *COOH. However, owing to the strong adsorption of CO on Mo single-atomic sites, these sites are often easily poisoned during CO_2RR. Additionally, the thermodynamically neutral nature of the hydrogen evolution reaction intermediate (H*) on Mo single-atomic sites suggests a strong competition from the HER as a side reaction. To address these two issues, Sun *et al.* co-deposited atomically dispersed Se atoms in the MoNC catalyst.[55] On one hand, Se atoms (electron configuration, $4s^2$ $4p^4$) have more valence electrons than C ($2s^2$ $2p^2$) and N atoms ($2s^2$ $2p^3$), allowing for more effective regulation of the d-electronic structure of Mo atoms. On the other hand, the additional valence electrons help repel water molecules from approaching the catalyst surface, hindering the HER progress (Fig. 3(e)). As a result, the obtained catalyst exhibited a FE_{CO} over 90% in the potential range from −0.4 to −1.0 V.

3.3 Construction of diatomic interface sites

As mentioned earlier, both coordination engineering and non-coordinating atom doping provide the atomic-site catalysts with rich adjustability. However, owing to the limitations of spatial constraints and electronic quantum states of single-atomic sites, the structures of these single-metal species stabilized on solid supports may not be suitable for catalyzing complex molecular transformations. Diatomic catalysts (DACs) almost perfectly inherit the advantages of single-atomic catalysts, also featuring near 100% utilization of their active atoms and the adjustable coordination environment of the metal centers. The design of diatomic interface sites is crucial for enhancing the rates, conversions, and selectivities of chemical reactions.[56] Additionally, the interatomic electronic interactions, co-adsorption, and synergistic catalytic effects of diatomic sites can surpass the limitations of intrinsic activity for single-atomic sites, thus showcasing the remarkable potential in the field of CO_2RR.

On the basis of these considerations, Jiao *et al.* constructed a Cu atom-pair catalyst (Cu-APC) from $Pd_{10}Te_3$ alloy nanowires.[14] The $Pd_{10}Te_3$ nanowire itself exhibits only minimal HER activity. In contrast, the synthesized Cu-APC demonstrates over 92% faradaic efficiency for CO production, with the competing HER almost completely suppressed. AC-HAADF STEM, XAS, and theoretical calculations collectively confirmed that the key catalytic sites are the $Cu_1{}^0$–$Cu_1{}^{x+}$ units (Fig. 4(a)), which play a crucial role in CO_2 reduction through a “diatomic-activating-bimolecular” mechanism. $Cu_1{}^{x+}$ acts as a Lewis acid, adsorbing water molecules, while $Cu_1{}^0$ acts as a Lewis base, adsorbing CO_2 molecules. The synergistic proton-coupled electron transfer between them greatly promotes the activation of CO_2. This work provides a novel and effective approach to constructing functional interfaces at the atomic level, and serves as an exemplary model for building diatomic catalytic interfaces for CO_2RR. Although positively charged Cu sites have been shown to significantly enhance the electrochemical CO_2RR to C_2 products, it is rather challenging to stabilize positively charged copper atoms under high cathodic potentials. To stabilize $Cu^{\delta+}$

sites, Zhang *et al.* designed and synthesized a $Pd^{\delta-}Cu_3N$ catalyst, which contains charge-separated $Pd^{\delta-}$–$Cu^{\delta+}$ atomic pairs.[57] Compared with Cu_3N, the $Pd^{\delta-}Cu_3N$ catalyst demonstrated a 14-fold increase in faradaic efficiency for C_2 products, reaching up to 78.2%. *In situ* characterizations and DFT calculations demonstrate that this diatomic site has an exceptional CO binding capability, and the synergistic effect between Pd and Cu plays a significant role in promoting the CO dimerization step for the production of C_2 products (Fig. 4(b)). This work presents a new strategy for the design and synthesis of diatomic interfaces and atomic modulation of relatively unstable $Cu^{\delta+}$ sites in CO_2RR.

The strategy of constructing diatomic interfaces has also been employed in catalyst design on N-doped C materials. The electronic effects between adjacent heteroatomic sites promote the formation and/or adsorption of specific intermediates, exhibiting CO_2RR activities superior to isolated monatomic counterparts.[58,59] For instance, Ren *et al.* reported the NiFe/NC catalyst with diatomic NiFe sites, which achieved a FE_{CO} above 90% within the range from −0.5 to −0.9 V *vs.* RHE, and the selectivity was barely changed after 30 h electrolysis (Fig. 4(c)), demonstrating an excellent durability.[60] Yi *et al.* synthesized CoCu/NC heterogeneous diatomic catalysts, where the CO selectivity remained above 95% across a broad range of current densities from 100 mA cm^{-2} to 500 mA cm^{-2} (Fig. 4(d)).[61] Previous effort was focused mainly on constructing heteronuclear diatomic sites on N-doped C supports. However, the synthesis of homonuclear diatomic sites using simple pyrolysis methods remains challenging. Hao *et al.* synthesized Ni_2NC catalysts through the co-pyrolysis of Ni–citric acid complexes adsorbed on carbon supports and dicyandiamide.[20] AC-HAADF-STEM and XAS spectroscopy confirmed the atomic dispersion of Ni atom pairs (Fig. 4(e)). In addition, *in situ* environmental scanning transmission electron microscopy (ESTEM) revealed that the formation of Ni_2 diatomic sites were mediated by Ostwald ripening. The hydroxyl-induced Ni diatomic site (Ni_2N_6OH) under reaction conditions served as an electron-rich active centres, significantly lowering the energy barrier for *COOH intermediate formation and *CO desorption. The authors further successfully synthesized a few other homonuclear diatomic sites such as Mn_2NC, Pd_2NC, and Zn_2NC using this synthesis method, demonstrating the universality of this strategy for the preparation of homonuclear diatomic sites.

What's more, different from single-atom catalysts, diatomic catalysts have demonstrated superior performance and advantages in C–C coupling due to the synergistic effect between adjacent metal sites.[62] For instance, Yang *et al.* reported a MOF with low-coordinated Cu diatomic sites, exhibiting exceptional current density of 0.9 A cm^{-2} and a high faradaic efficiency of 71% for C_2 products.[63] *In situ* characterization and theoretical

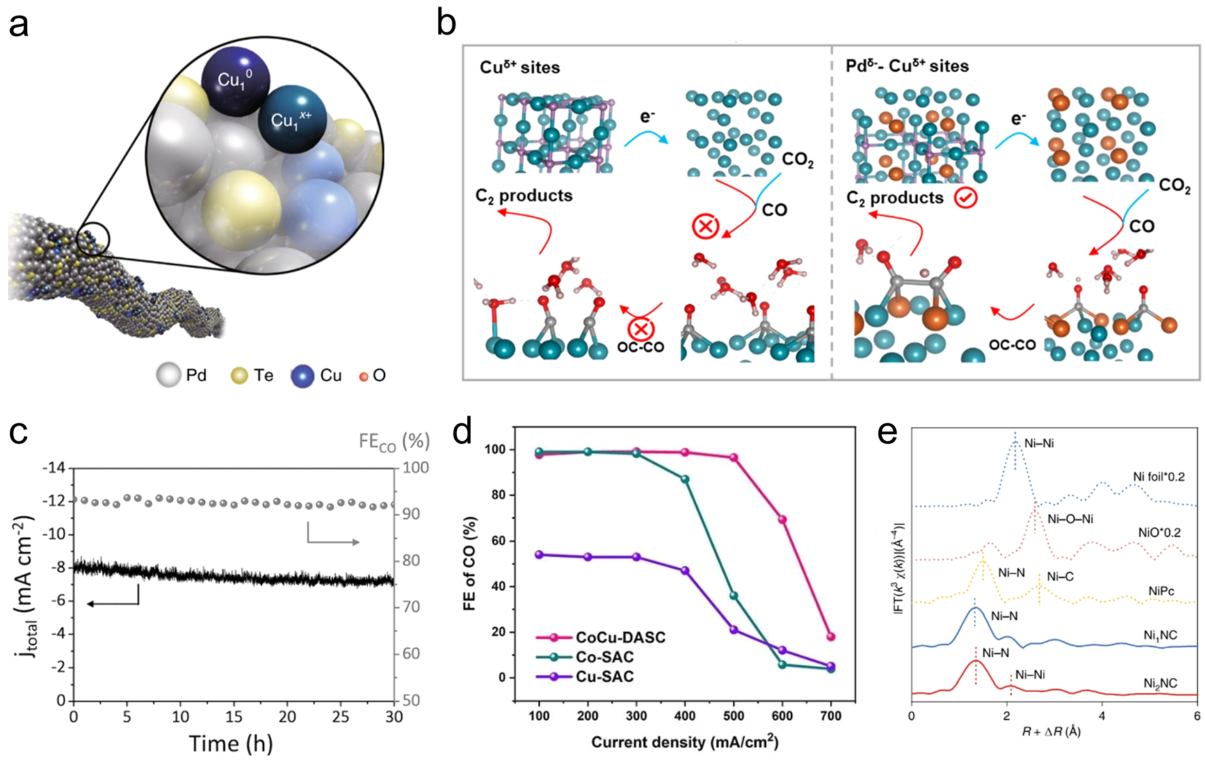

Fig. 4 (a) Schematic diagram of the Cu atom pair anchored on $Pd_{10}Te_3$ nanowires. Reproduced with permission from ref. 14. Copyright 2019, Springer Nature. (b) Schematic diagram of the catalytic CO_2RR process to C_2 products on $Pd^{\delta-}$–$Cu^{\delta+}$ atom pairs. Reproduced with permission from ref. 57. Copyright 2023, American Chemical Society. (c) Stability test for the Ni/Fe–N–C catalyst. Reproduced with permission from ref. 60. Copyright 2019, Wiley-VCH. (d) FE_{CO} of CoCu-DASC, Co-SAC and Cu-SAC. Reproduced with permission from ref. 61. Copyright 2022, Wiley-VCH. (e) Fourier transforms (FT) of k^3-weighted Ni K edge EXAFS experimental data for Ni_2NC, Ni_1NC, NiPc, NiO and Ni foil. Reproduced with permission from ref. 20. Copyright 2022, Springer Nature.

calculations revealed that the key to C–C coupling at the diatomic sites is the stable adsorption of two *CO intermediates on the adjacent Cu sites. Furthermore, to enhance the selectivity towards specific C_2 products, Zhao *et al.* rationally designed a novel heterometallic Sn⋯Cu dual-site catalyst.[64] The active centers of this catalyst are defined as SnN_2O_2 and CuN_4 sites bridged by N atoms. Mechanistic studies indicated that due to the higher oxygen affinity of the SnN_2O_2 sites, the heterometallic Sn⋯Cu dual sites are more favorable for asymmetric C–C coupling between *CO and $*OCH_2$, leading to the predominant production of ethanol. Ultimately, this catalyst achieved a current density of 68 mA cm^{-2} at a low potential of −0.57 V (*vs.* RHE), with an $FE_{ethanol}$ of 56%, and maintained considerable stability. In summary, the development of diatomic catalysts provides a potential pathway for efficient C–C coupling in CO_2RR. These studies provide reliable support for understanding the interfacial information of diatomic catalysts.

4. Surface/interface engineering for metal catalysts

Due to the complex surface structure and relatively concentrated active sites, metal catalysts exhibit significant selectivity towards various products of CO_2RR. And the controllable synthesis of nanocrystals provides great convenience for the modelization of metal catalysts, facilitating the exploration and optimization of their surface structures. After years of research, many metal catalysts demonstrate high catalytic activity, enabling efficient conversion of CO_2 to value-added products at relatively low overpotentials, which is crucial for energy efficiency. For example, Pd-, Ag-, and Au-based catalysts are effective in catalyzing the conversion from CO_2 to CO; Bi- and Sn-based catalysts can help selectively reduce CO_2 to HCOOH; Cu is widely used for the high-selectivity conversion of CO_2 into various multi-carbon products.[65–70] However, the electrocatalytic CO_2RR system is rather complex, with many reaction pathways involving different intermediates. Because of the formation of similar surface adsorption bonds, the binding energies of different intermediates are correlated to each other, a phenomenon known as the scaling relationship.[71] Simple metal catalysts usually have a uniform surface structure, making it difficult to achieve specific adsorption of particular intermediates, resulting in low intrinsic catalytic activities. Therefore, it is necessary to engineer the surfaces/interfaces of metal catalysts to decouple the binding of different intermediates, thereby improving the selectivity and activity for CO_2RR.

4.1 Facet engineering and molecular modification

The different facets of nanocrystal catalysts have distinct electronic structures, leading to varying adsorption strengths for different CO_2RR intermediates, which significantly impacts catalytic performance. Therefore, the most straightforward method to regulate metal catalysts is to maximize the proportion of dominant crystal facets in the nanostructure, thus achieving more effective adsorption of specific intermediates. Numerous studies have confirmed the effectiveness of this strategy. Compared with octahedral facets exposing (111) crystal planes and truncated ditetragonal prisms exposing (310) crystal planes, rhombohedral facets exposing (110) crystal planes in gold nanocrystals exhibit higher CO_2RR activity and selectivity, especially at low overpotentials.[66] Liu *et al.* synthesized triangular Ag nanoplates, and demonstrated that the Ag(100) facet significantly lowers the required Δ*G* for the formation of COOH*.[67] Triangular Ag nanoplates, with more exposed Ag(100) crystal planes compared with similarly sized Ag nanoparticles and bulk Ag, show an enhanced current density, significantly improved faradaic efficiency (96.8%) for CO and energy efficiency (61.7%), as well as a considerable stability. For the same crystal facet, the performance of electrocatalysts can also be influenced by the differences in electronic structure resulting from surface strain. Huang *et al.* demonstrated that tensile strain on the surface of Pd icosahedra (Fig. 5(a)) shifts the d-band center upward, enhancing the adsorption of crucial intermediate COOH* and thereby achieving higher CO_2RR activity to CO than Pd octahedra do.[17] Facet control is also important in CO_2RR to multi-carbon products. With the dominant exposed Cu(100) and Cu(111) crystal facets, metal copper nanocrystals derived from cuprous chloride precursors can effectively adsorb key $*C_1$ and $*C_2$ intermediates, demonstrating a considerable yield for propylene (Fig. 5(b)).[16]

Organic small molecules/polymers have great potential in further regulating the surface structure of metal catalysts. On one hand, molecular modification can improve the adsorption of intermediates on the catalyst surface. Li *et al.* deposited a series of differently substituted *N*-arylpyridinium salts on a porous polytetrafluoroethylene gas diffusion layer, forming an

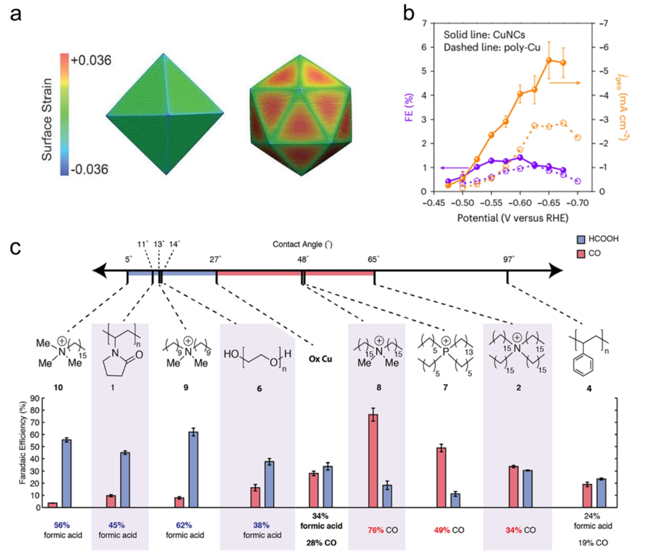

Fig. 5 (a) Schematic diagram of the surface strain fields of the Pd icosahedron and octahedron. Reproduced with permission from ref. 17. Copyright 2017, Wiley-VCH. (b) Partial current density and FE for CO_2RR to propylene on polycrystalline copper and CuNCs. Reproduced with permission from ref. 16. Copyright 2023, Springer Nature. (c) The contact angles, FE_{CO} and FE_{HCOOH} of organic molecular modified Cu surfaces. Reproduced with permission from ref. 73. Copyright 2019, American Chemical Society.

organic–metal interface with a sputtered Cu layer.[72] This strategy effectively enhanced the stability of 'atop-bound' CO, which is the key intermediate in CO_2RR to ethylene. In liquid-electrolyte flow cell tests, this system exhibited a 72% ethylene faradaic efficiency and a partial current density of 230 mA cm^{-2}. On the other hand, organic molecule/polymer modification can regulate the microenvironment (including local pH, interfacial water *et al.*) near the catalyst interface, thus optimizing the mass transport and local concentrations of carbon dioxide and water. Buckley *et al.* investigated the effects of a range of polymers and molecular modifiers on the selectivity of Cu catalysts for CO_2RR.[73] They found that protic polymers could provide abundant protons for Cu, enhancing the HER activity. Among aprotic polymers, cationic hydrophobic polymers were found to improve the selectivity for CO, while hydrophilic polymers promoted the formation of formic acid (Fig. 5(c)). Similarly, imidazolium-based ionomers were shown to regulate the competing HER on Ag surfaces, thereby controlling the efficiency of CO_2RR.[74] Surface-bound dihexadecyldimethylammonium bromide greatly increased the faradaic efficiency for CO (from 25% to 97%) by promoting the mass transport of carbon dioxide and water near the Ag foil surface.[75]

Metal catalysts, especially copper-based catalysts, often exhibit low selectivity and poor stability owing to severe surface restructuring. *In situ* reduction of Cu(II)Pc precursors on conductive carbon nanoparticles (CNP) can constrain the size of Cu clusters, generating low-coordination copper sites. However, within one hour, the faradaic efficiency of CO_2RR to methane rapidly decreases (from 46% to 25%) because of the continuous leaching and aggregation of copper ions. To address this issue, Fan *et al.* prepared ligand-modified CuPc/CNP composite catalysts.[76] Ethylenediaminetetraacetic acid (EDTA), with its strong coordinating ability, captures and stabilizes free copper ions, thereby preventing the leaching and growth of copper clusters, and greatly enhancing the catalyst's stability. This strategy demonstrates that surface modification with organic molecules can also regulate the catalytic performance by controlling the structure evolution of metal catalysts.

4.2 Metal–metal interface

In contrast to single-component metal catalysts, the catalytic performance of bimetallic catalysts is highly dependent on the atomic distribution. The interactions occurring at the interface of the two metals are significantly different from those of bulk metals. The effect could alter the adsorption energy of intermediates or suppress competing reactions, and thus constructing bimetallic catalysts provide an effective and promising approach to modulating the selectivity and activity of CO_2RR.[71] *Ab initio* calculations have identified that the Sn/Bi bimetallic interface would favor HCOOH formation. On the basis of this result, Ren *et al.* constructed a rich Sn–Bi interface on three-dimensional highly porous carbon fabrics (3D CF) through *in situ* electrodeposition (ED) and evolution under CO_2RR conditions.[68] Compared with pure Sn and Sn–Bi bulk alloy, this bimetallic interface structure has proven to enhance the p-band center of Sn because of charge transfer from Sn to Bi (Fig. 6(a)). This weakens the Sn–C hybridization of competing COOH* adsorption, while strengthening the Sn–O hybridization of HCOO* adsorption. The resulting Sn–Bi bimetallic catalyst exhibits a faradaic efficiency >90% for formic acid over a wide potential window (from −0.74 to −1.14 V *vs.* RHE), with a partial current density up to 140 mA cm^{-2}, and maintains its stability for 160 h. Similarly, Wu *et al.* successfully synthesized a Sn–Bi-based bimetallic aerogel with abundant interfaces and channels, which demonstrated excellent conversion rates for CO_2RR to formic acid.[69]

Copper is the only known metal capable of catalyzing the generation of multi-carbon products from CO_2RR with notable efficiencies. However, copper catalysts are often limited by poor selectivity.[77] Compared with pure copper, copper-based bimetallic materials can optimize the reaction kinetics through charge transfer, spillover effects, and other mechanisms, thereby improving the selectivity of CO_2RR.[11] Unlike Cu, the overpotential for CO_2 reduction over Pd systems is lower, and CO or formic acid is typically the main product. However, by controlling the metal ratio of PdCu aerogels, Lu *et al.* prepared a $Pd_{83}Cu_{17}$ aerogel catalyst with a faradaic efficiency up to 80.0% for methanol production, with a current density of 31.8 mA cm^{-2}. The excellent catalytic performance of this aerogel is attributed mainly to the synergistic effects between Pd^0 and Cu^I, which facilitates the efficient adsorption and stabilization of the $^{\bullet}CO_2^-$ radical anions at the interface.[70]

In addition to C_1 products, some metal–metal interfaces are believed to promote the generation of multi-carbon products through a tandem catalysis mechanism. Morales-Guio *et al.* employed physical vapor deposition to deposit gold nanoparticles on the surface of polycrystalline copper foil, and obtained an Au/Cu bimetallic catalyst.[78] Catalytic testing and characterization results indicate that the gold nanoparticles could increase the local concentration of CO at the Au/Cu interface, leading to CO spillover from the Au surface to the Cu surface. This effectively increases the probability of C–C coupling on the Cu surface. The catalyst exhibits significantly enhanced efficiency in converting carbon dioxide to >2e^- reduction products, surpassing that of individual gold or copper by more than two orders of magnitude. Employing high-resolution transmission electron microscopy characterization, Zhu *et al.* revealed the reconstruction/phase transition of bimetallic electrocatalysts during the tandem CO_2RR.[79] The oxidation/reduction of Cu during electrocatalysis drives the transition from phase-separated bimetallic AuCu to alloy-supported core–shell nano-clusters (Fig. 6(b)). *In situ* infrared spectroscopy experiments in combination with theoretical simulations further confirm that the accumulation of *CO at the metal–metal interface is a key factor in the continuous production of C_{2+} alcohols.

In contrast to Au–Cu bimetallic catalysts, the primary product of CO_2RR at the Ag–Cu interface is ethylene. The key structure responsible for the enhancement in the faradaic efficiency for C_2H_4 is also the Ag–Cu interface. The Cu/Ag mass ratio has a significant impact on the catalytic performance. Compared with Cu nanoparticles of a similar size and shape,

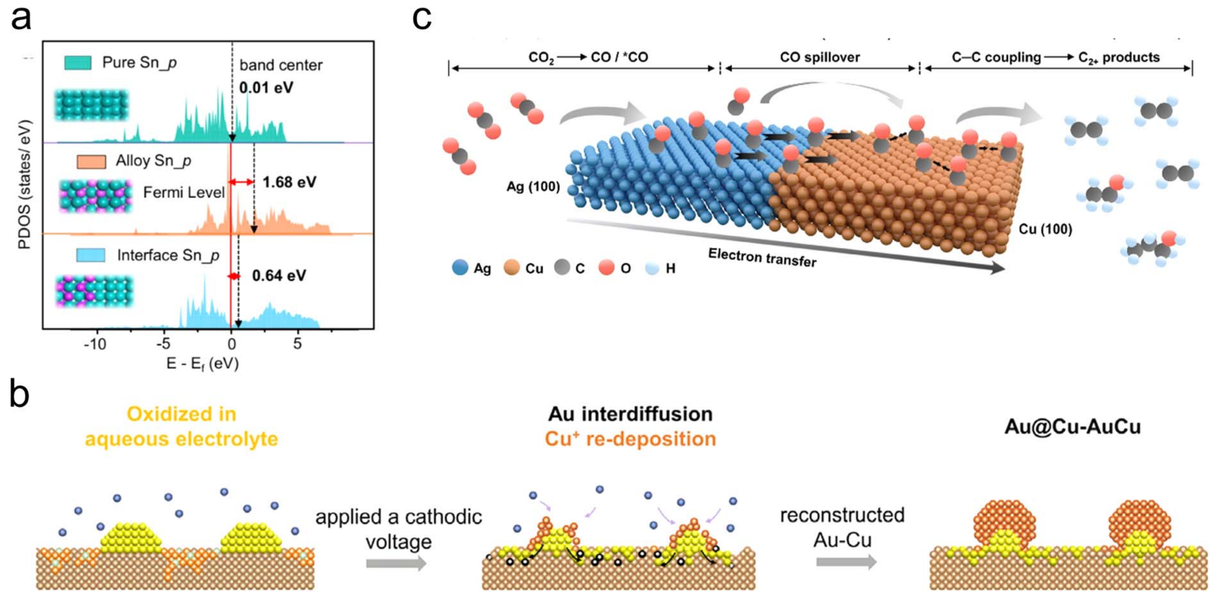

Fig. 6 (a) Partial density of states (PDOS) of Sn 5p orbitals of interface Sn, alloy Sn and pure Sn. Reproduced with permission from ref. 68. Copyright 2022, Springer Nature. (b) Schematic diagram of the proposed structural reconstruction and phase transformation of Au–Cu catalyst during CO_2RR. Reproduced with permission from ref. 79. Copyright 2022, Elsevier. (c) Schematic diagram of a plausible CO_2RR mechanism on Ag_{65}–Cu_{35} JNS-100 catalyst. Reproduced with permission from ref. 81. Copyright 2022, Wiley-VCH.

the synthesized Ag_1–$Cu_{1.1}$ nanodimers demonstrated a 3.4-fold increase in the FE for ethylene and an overall 2-fold enhancement in CO_2RR activity.[80] For Ag–Cu catalysts, the improvement in performance is attributed to electron transfer at the metal–metal interface and CO spillover (Fig. 6(c)).[81] In order to further investigate the dynamic catalytic sites of Ag–Cu catalysts during CO_2RR and achieve a rational design of AgCu catalysts, Chen *et al.* synthesized mixed and phase-separated AgCu nanoparticles on a carbon paper electrode.[82] Through time-sequential electron microscopy and elemental mapping, the migration behavior of Cu in AgCu under CO_2RR conditions was observed for the first time, ultimately leading to the identification of thermodynamically stable Ag-rich and Cu-rich grains, namely $Ag_{0.88}Cu_{0.12}$ and $Ag_{0.05}Cu_{0.95}$. Additionally, operando high-energy-resolution X-ray absorption spectroscopy confirmed that the metallic state of Cu in AgCu serves as the catalytically active site during the CO_2RR process. The above-mentioned research is crucial for a more in-depth understanding of the structure–activity relationship of bimetallic catalysts, and it is beneficial for guiding the design of more efficient Ag/Cu catalysts.

4.3 Alloying and heteroatom doping

Alloying provides a novel approach to disrupting the scaling relationship. Interactions with heteroatoms can induce geometric and/or electronic effects to alter surface adsorption properties and reactivity.[11] For example, the high-index (211) face of face-centered cubic (fcc) Au exhibits superior current density for the electrochemical CO_2RR to CO, approximately 20 times higher than the low-index (100) face of fcc Au. However, owing to the thermodynamically unfavorable properties, further optimization of interface architecture, composition, and defects is still required to achieve stable and superior catalytic performance. Recently, Zhou *et al.* synthesized hexagonal close-packed (2H-type)/fcc-heterophase AuCu alloy nanostructures using a simple wet-chemical method.[83] *In situ* differential electrochemical mass spectroscopy (DEMS) and attenuated total reflection Fourier-transform infrared spectroscopy (ATR-FTIR) demonstrate that the unique structural features of the synthesized 2H/fcc $Au_{99}Cu_1$, with appropriate copper alloying on high-index surfaces, play a crucial role in enhancing CO_2RR performance. For metallic species that are difficult for alloying, a controllable electrodeposition approach is typically used to construct alloy catalysts. For example, alloying metals with high oxygen affinity into Cu can enhance the binding of O. This strategy can increase the adsorption energy of $*CH_xO$ and improve methane production. The La_5Cu_{95} synthesized using this method exhibited high performance in a flow cell, with a faradaic efficiency for methane of 64.5% and a partial current density of 193.5 mA cm^{-2}.[84] Similarly, using a co-electrodeposition method with suppressed galvanic replacement, Qi *et al.* prepared an AgCu alloy catalyst with exceptional selectivity for 2-propanol.[85] Dispersed Ag atoms in Cu could weaken the surface binding of intermediates in the middle position of the alkyl chain and strengthen the C–O bonds. Furthermore, it is worth noting that GaCu alloy not only exhibits superior catalytic activity for CO_2RR,[86] but also greatly enhances the stability of the catalyst because Ga could suppress Cu oxidation at open-circuit potential and impart significant electronic interactions with Cu.[87]

In order to fundamentally understand the atomic structure of active sites and thereby achieve more precise control over alloy catalysts, Wang *et al.* synthesized a series of PdAu catalysts with varying Pd content (Fig. 7(a)).[88] The study reveals a non-linear relationship between the catalytic activity for CO_2 reduction to CO and the Pd content, which is due to the different adsorption energies of CO and carboxyl on Pd sites in different size ensembles. Pd dimers, in particular, exhibited the optimal catalytic performance as they could activate CO_2 with lower energy barriers and avoid strong binding with CO intermediates. Consequently, single-atom alloy (SAA) catalysts have been developed to optimize the catalytic performance for CO_2RR by controlling the catalyst's electronic structure to regulate the adsorption of intermediates.[89] For instance, Cao *et al.* reported that the BiCu-SAA could effectively catalyze CO_2RR to multi-carbon (C_{2+}) products due to enhanced CO_2 adsorption, $^*CO_2$ protonation and C–C coupling (Fig. 7(b)).[90] Selective production of formate *via* CO_2RR using Cu catalysts is often challenging because it is rather difficult to suppress the C–C coupling process. CO_2 molecules become adsorbed and activated on the catalyst surface, forming HCOO* or COOH* intermediates. The former is a key intermediate for formate production, whereas the latter (and its subsequent CO/CO* derivatives) leads to C_1 and C_{2+} products other than formate. Therefore, for the selective conversion of CO_2 to formate over Cu-based catalysts, it is essential to maximize the generation of HCOO* intermediates rather than COOH*. In this regard, Zheng *et al.* reported a Pb_1Cu single-atom alloy catalyst that can convert CO_2 into formate with a faradaic efficiency of ~96% and a partial current density of over 1 A cm^{-2} (Fig. 7(c)).[91] The Pb_1Cu electrocatalyst converts CO_2 to formate at the modulated Cu sites rather than on isolated Pb. Both *in situ* spectroscopic evidence and theoretical calculations indicate that the atomically dispersed Pb lowers the energy barrier for the first protonation step of the CO_2RR to HCOO*, thus achieving efficient formate production.

Compared with metallic dopants, non-metal dopants, such as B, S, and halogens, are expected to exhibit greater modulation capabilities on the electronic structures of metal catalysts on account of their higher electronegativity.[92–95] In copper catalysts, surface $Cu^{\delta+}$ sites are considered active for CO_2RR. Previously, $Cu^{\delta+}$ has been introduced by employing oxygen-containing species, derived from copper oxide catalysts. However, under CO_2RR conditions, especially at high cathodic potentials required for the formation of C_2 products, $Cu^{\delta+}$ species can be easily reduced to Cu^0, resulting in poor stability of the copper catalysts. Theoretical calculations indicate that boron is more prone to diffuse into the subsurface of Cu(111) crystal planes, whereas oxygen tends to remain on the surface. This suggests that boron doping has the potential to enhance the stability of $Cu^{\delta+}$ species at high potentials and thus improve the stability of copper catalysts. Additionally, compared with pure copper, the d-band center of copper atoms near boron is shifted away from the Fermi level, indicating a greater positive charge on the neighboring copper atoms. This results in

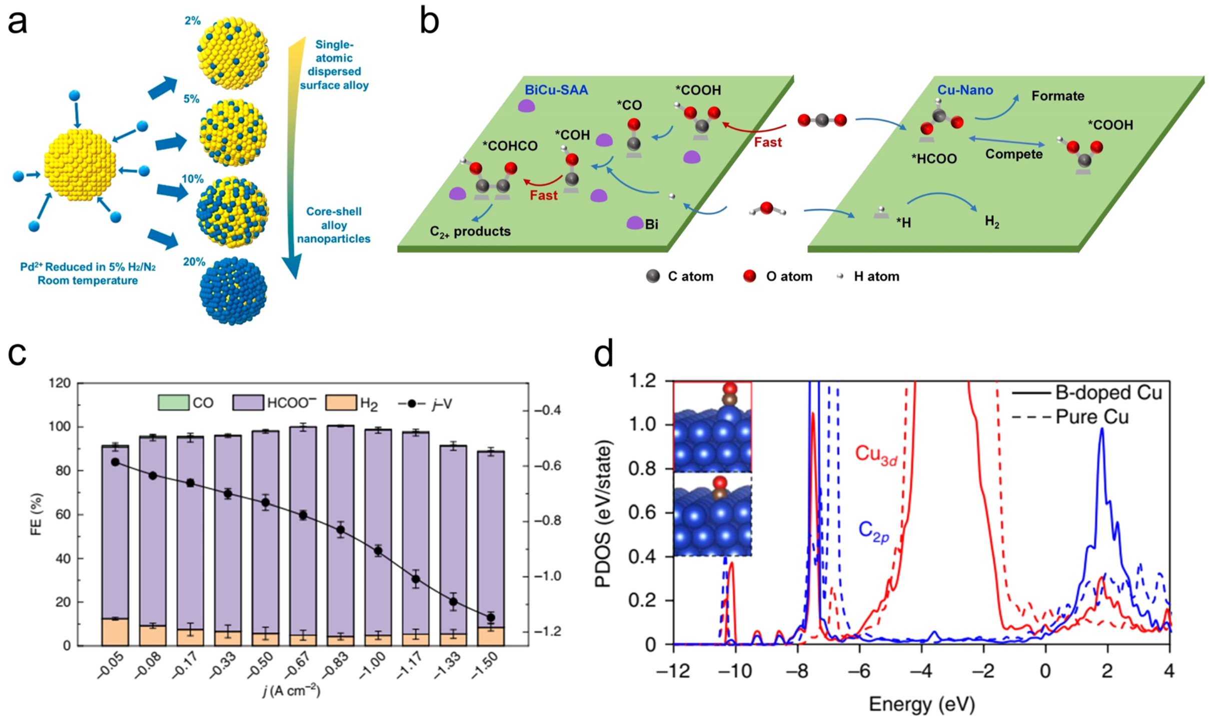

Fig. 7 (a) Schematic diagram of the preparation process for the Pd@Au nanoparticles with different dose of Pd. Reproduced with permission from ref. 88. Copyright 2019, American Chemical Society. (b) Schematic diagram of the proposed reaction mechanism of CO_2RR on the BiCu(111)-SAA and Cu(111)-Nano. Reproduced with permission from ref. 90. Copyright 2023, Wiley-VCH. (c) FEs of all CO_2RR products at different current densities and the corresponding *j*–*V* curve of Pb_1Cu catalyst. Reproduced with permission from ref. 91. Copyright 2021, Springer Nature. (d) Partial density of states (PDOS) of Cu_{3d} and C_{2p} orbitals in boron-doped copper and pure copper catalysts. Reproduced with permission from ref. 92. Copyright 2018, Springer Nature.

stronger binding energy of CO on boron-doped copper surfaces (Fig. 7(d)). On the basis of these considerations, Zhou *et al.* synthesized boron-doped copper catalysts, which exhibited approximately 80% C_2 faradaic efficiency and retained the stability for over 40 hours.[92] Furthermore, halogen atoms have even higher electronegativities and can enhance CO adsorption by increasing surface $Cu^{\delta+}$ sites. Ma *et al.* synthesized a series of halogen-doped Cu catalysts, among which fluorine-modified Cu demonstrated the highest catalytic activity, with a current density of up to 1.6 A cm^{-2} and 80% C_{2+} (mainly ethylene and ethanol) faradaic efficiency.[93] This is attributed to the ability of halogen-modified Cu surfaces to activate water molecules and facilitate *CHO intermediate formation; on the basis of these findings, the team proposed a novel hydrogen-assisted C–C coupling mechanism.

5. Surface/interface engineering for metal/oxide catalysts

The unique oxidation state structure, abundant surface acidic sites, and variable valence capability of oxides provide a broad platform for tailoring the surface/interface structures of catalysts, thereby offering immense new opportunities to enhance catalytic performance. For instance, by tailoring the meta/oxide (M/O) interface, one can obtain stable adsorption sites for key reaction intermediates, thereby facilitating the activation of CO_2 and the selective generation of specific products.[21,96] Recent studies have also indicated that some oxidation states of active sites, which are difficult to stabilize during CO_2RR, can be effectively stabilized through the design of M/O interface.[97,98] In this section, considering the diversity in design approaches, we categorize metal/oxide catalyst interfaces into two major groups: namely, homonuclear M/O interfaces and conventional M/O interfaces, and discuss them separately.

5.1 Homonuclear M/O interfaces

In the design of homonuclear M/O interfaces, particular attention needs to be focused on the unique active interface sites formed between the metal active centers and their corresponding oxidized-state sites. This synergistic interaction could potentially promote the activation of CO_2 and enhance the selectivity. Constructing homonuclear M/O interfaces can be achieved by two means: one involves the preparation of a metal (such as Cu,[99] Co,[100] *etc.*) and the subsequent implementation of an *in situ* oxidation method to convert the surface metal atoms into their corresponding metal oxides. The other means is to first synthesize compounds with a certain oxidation state (such as metal oxides,[101,102] metal phosphates,[103] *etc.*), and then obtain homonuclear M/O interfacial sites through an *in situ* electrochemical reconstruction process.

Xie *et al.* conducted a series of investigations on atomic layer catalysts related to Co for the conversion of CO_2 into formate.[100] They prepared two types of catalysts, each consisting of four atomic layers (pure cobalt metal and a domain where cobalt metal coexists with cobalt oxide), aiming to elucidate the impact of their inherent oxides on electrocatalytic activity. The team found that the surface Co atoms in the atomic-thin layers exhibited a higher intrinsic activity and selectivity for formate compared with the surface Co atoms in bulk samples. Additionally, the intrinsic activity of partially oxidized atomic layers was further enhanced. This research underscores the critical role of atomic-scale structures and the presence of oxides on metal catalysts in intrinsic activity and selectivity. Copper, as one of the most intriguing catalysts on account of its unique capability in producing hydrocarbons, has been widely studied for its M/O interface. Chou *et al.* conducted *in situ* SEIRAS to investigate the interaction of different oxidation states of Cu surface with surface intermediates.[99] They observed that electrodeposited copper electrodes exhibited a higher Cu^+ content, with surface CO intermediates predominantly existing in the configuration of top adsorption (CO_{atop}). During further reduction processes, CO_{atop} led to the generation of C_1 hydrocarbon products, such as methane. At the oxidized state surface of Cu^0 bridge-bonded CO (CO_{bridge}) are readily formed, suppressing the formation of hydrocarbon products. In contrast, Cu electrodes treated with cyclic voltammetry (CV) exhibited a coexisting M/O interface of Cu(I) and Cu(0). During CO_2RR, this interface resulted in the formation of both CO_{atop} and CO_{bridge}, thus enhancing the selectivity for C_2 products (Fig. 8(a and b)).

Oxide-derived catalysts (OD-catalysts) represent an important category of catalysts for CO_2RR and serve as a crucial means to obtain homonuclear M/O interfaces. Kanan *et al.* systematically investigated a range of OD-catalysts, such as OD-Cu, OD-Au, and OD-Sn, for CO_2RR, revealing enhanced electrochemical activity and selectivity.[101,102,104,105] As the research progressed, scientists developed other electrochemical reconstruction-derived catalysts to obtain homonuclear M/O interfaces, including metal phosphate derivatives, metal silicate derivatives, and more, aiming for more stable electrochemical active M/O interfaces and superior performances.[103,106,107] As mentioned earlier, the synergistic effect between Cu^0 and Cu^+ promotes the generation of C_2 products. However, obtaining stable Cu^+ species during the CO_2RR process has been a daunting challenge. To address this issue, Yuan *et al.* synthesized $CuO/CuSiO_3$ composite catalysts, where Cu^{2+} species were *in situ* reduced to Cu^0 and Cu^+ during the electrochemical process.[106] By adjusting the loading amount of Cu, the authors achieved continuous tunability of the Cu^0/Cu^+ ratio. During the CO_2RR process, Cu^0 facilitated CO_2 activation by lowering the thermodynamic activation energy barrier, whereas Cu^+ enhanced the adsorption of the intermediate *CO. The synergistic interaction at this M/O interface enhanced the dynamics of C–C coupling. Notably, the catalyst with 20% $Cu/CuSiO_3$ exhibited a remarkable 51.8% selectivity for C_2H_4. Recent studies have indicated that asymmetric coupling between *CO and *CHO or *COH has lower energy barriers than direct *CO–*CO coupling.[108–110] The key challenge lies in designing interface sites to achieve asymmetric coupling. Apart from the extensively studied Cu^+ species, Cu^{2+} species with a higher oxidation state exhibit structural features that facilitate the binding of CO or H_2O.[111,112] This enhanced CO adsorption is expected to promote further protonation of *CO to

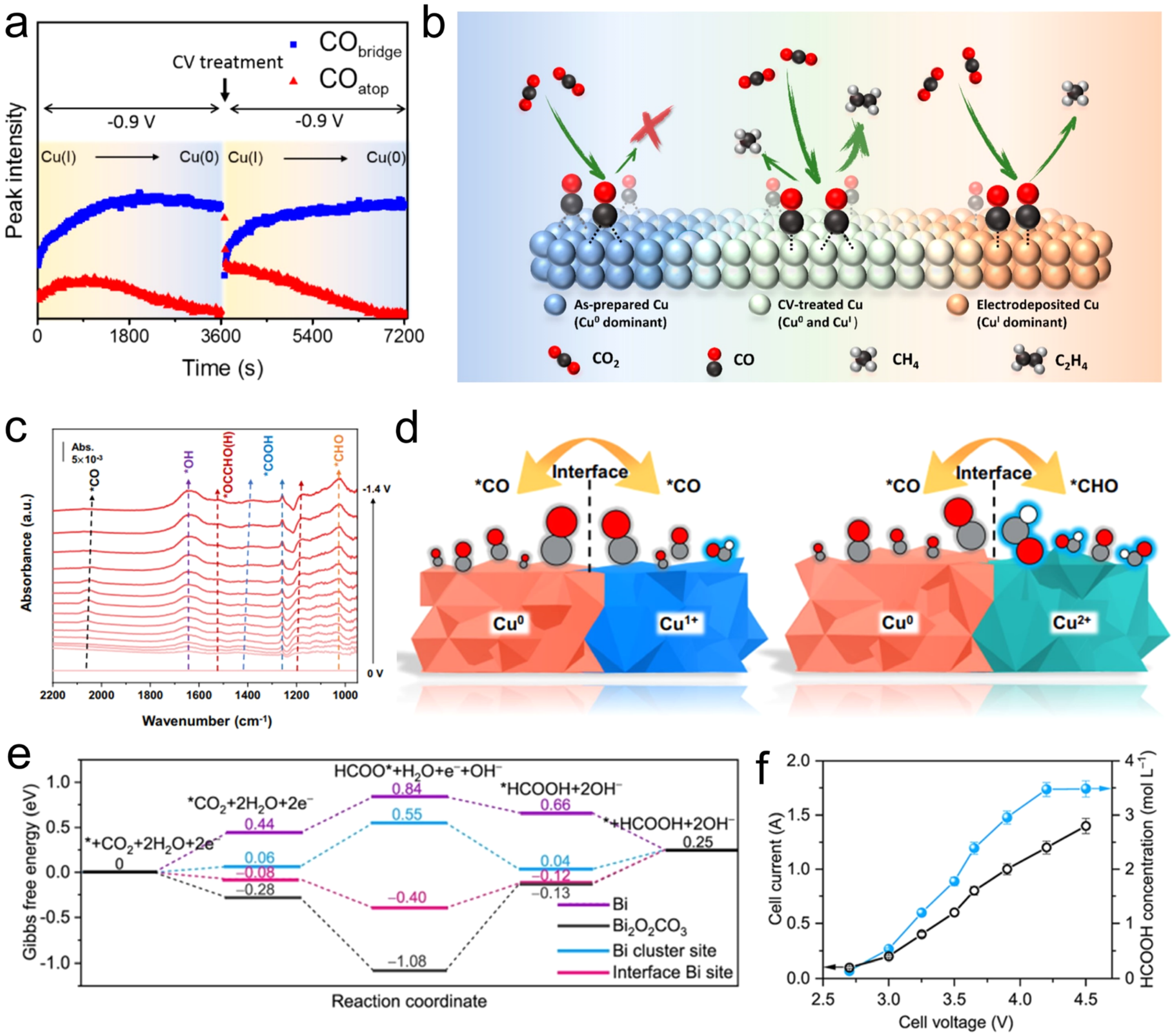

Fig. 8 (a) Time dependence of the CO_{bridge}- and CO_{atop}-associated peak intensities at −0.9 V. (b) Schematic Illustration of the CO_2RR on the Cu surface. Reproduced with permission from ref. 99. Copyright 2020, American Chemical Society. (c) *In situ* SEIRAS spectra of the $Cu_3(PO_4)_2$ in 0.1 M $KHCO_3$ electrolyte in real-time condition. (d) Schematic diagram of different intermediates on the Cu^0/Cu^+ and Cu^0/Cu^{2+} interfaces. Reproduced with permission from ref. 103. Copyright 2023, Springer Nature. (e) Gibbs free energy diagram for CO_2RR to HCOOH on Bi, $Bi_2O_2CO_3$, Bi cluster site of $Bi_3/Bi_2O_2CO_3$, and interfacial Bi site of $Bi_3/Bi_2O_2CO_3$. (f) The total current and the concentration of formic acid at different cell voltages in the solid-electrolyte cell. Reproduced with permission from ref. 114. Copyright 2023, Wiley-VCH.

*CHO (or *COH). Thus, the rational design of Cu^0/Cu^{2+} interface sites holds promise for facilitating the CO–CHO coupling process. However, obtaining stable Cu^{2+} during the CO_2RR is rather difficult. To address this issue, Zhang *et al.* utilized the Materials Project Database and DFT calculations, and screened 83 compounds containing Cu^{2+} species, eventually identifying Cu^{2+} phosphorus oxysalts (CuPO) as the most promising candidate for stable Cu^0/Cu^{2+} interface under electroreduction conditions.[103] Subsequently, the team experimentally synthesized the CuPO catalyst, which exhibited a faradaic efficiency of 90.9% for C_{2+} products with a C_{2+} partial current density of over 300 mA cm^{-2} in a flow cell. *In situ* SEIRAS further demonstrated that Cu^{2+} sites favored the formation of *CHO, which could be readily coupled with *CO on the Cu^0 surface to form *OCCHO intermediates, thereby achieving efficient CO_2-to-C_{2+} conversion (Fig. 8(c and d)).

The design of homonuclear M/O interface has been widely applied to other metal active sites as well. For instance, bismuth compounds (such as Bi_2O_3, Bi-MOF) often undergo a dynamic restructuring process from Bi^{3+} to $Bi_2O_2CO_3$ during the CO_2RR.[34,113] This process becomes more pronounced in alkaline-electrolyte flow cells, and the inherent capability of oxidative state retention provides a foundation for designing the Bi/Bi^{3+} interface.[35] In their theoretical investigations, Lin *et al.* found that the activation of CO_2 and the formation of HCOO* proceed slowly on the surface of metallic Bi, despite the favorable energy landscape for the subsequent reduction to *HCOOH and its subsequent desorption. In the case of $Bi_2O_2CO_3$, strong Coulomb interactions between CO_2 and positively charged surface Bi atoms facilitate the activation of CO_2 and the subsequent formation of HCOO*, but the subsequent protonation of HCOO* and the desorption of *HCOOH become challenging. In light of this, the team designed and prepared a stable Bi^0 cluster and $Bi_2O_2CO_3$ nanosheets as the active phase by using Bi_2S_3 as a precursor in an alkaline flow cell.[114] Experimental and theoretical results indicate that this Bi^0/Bi^{3+} interface exhibits optimized CO_2 activation and subsequent intermediate protonation capabilities, demonstrating excellent selectivity for formate (Fig. 8(e)). It achieves a 93% selectivity for formic acid at a high current density of 2 A cm^{-2}, and the electrochemical stability can be maintained for over 100 hours. Furthermore, employing solid-state electrolyte devices, the team successfully achieved continuous production of 3.5 mol L^{-1} pure formic acid (Fig. 8(f)). These results indicate that establishing homonuclear M/O interfaces to achieve synergistic interactions between metals and their oxidized species is a highly promising strategy for the design of advanced CO_2RR catalysts.

5.2 Conventional M/O interfaces

In contrast to homonuclear M/O interfaces, the design of conventional metal/oxide catalysts typically involves the composite of active metals with electrochemically relatively inert metal oxides to regulate the properties of the M/O interfaces. This approach has achieved significant success in thermocatalytic CO_2 hydrogenation.[115,116] In recent years, with the continuous development of electrocatalytic CO_2RR technology, researchers have come to realize that constructing suitable M/O interface can effectively stabilize reactive species or regulate processes such as the adsorption and desorption of reaction intermediates.[21,117] This, in turn, directly influences the activity and selectivity of CO_2RR.

Ceria has been widely employed in constructing active M/O interface for CO_2RR by virtue of its unique physicochemical properties, including outstanding stability, and tunable oxidation states. Liu *et al.* synthesized a CeO_2–SnO_2 heterostructure catalyst using a facile electrospinning method, and achieved a maximum formate partial current density of 500 mA cm^{-2} and a faradaic efficiency of 87.1% during CO_2RR.[118] Through *in situ* SEIRAS and XPS analysis, the team proposed a dynamic CeO_2-mediated $Sn^0/Sn^{\delta+}$ redox cycling mechanism (Fig. 9(a)). The oxygen vacancies generated on the CeO_2 surface facilitate water decomposition to produce *OH and *H species. The former oxidizes Sn^0 to active $Sn^{\delta+}$, promoting the conversion of CO_2 to a crucial intermediate, *OCHO, with the assistance of the *H. The strategy of utilizing CeO_2 to stabilize the oxidation state of active centers has also been applied to stabilize Cu^{2+} species by Qiao's research group.[98] The majority of Cu-based catalysts would undergo electrochemical reduction from Cu^{2+} to Cu^0 or Cu^+, often accompanied by phase restructuring and the formation of new active centers. The team employed CeO_2 as a sacrificial component to protect the Cu^{2+} active species (Fig. 9(b)). Through *in situ* Raman spectroscopy experiments, they observed a significant increase in Ce^{3+} concentration in Cu–CeO_x after CO_2RR, demonstrating that electrons would preferentially reduce Ce^{4+} to Ce^{3+} in Cu–Ce-O_x. Simultaneously, the newly generated Ce^{3+}/Ce^{4+} pairs act as a conductive network, enhancing the overall conductivity of the solid solution, accelerating electron transfer, and thereby inhibiting the electron accumulation at Cu^{2+} sites and preventing their self-reduction. As a result, the stabilized Cu^{2+} enhances CO adsorption and further hydrogenation to produce CH_4 rather than dimerization to form C_2 products. Additionally, M/O between metals such as Au, Bi, Cu, and ceria has shown significant potential in promoting the adsorption and activation of CO_2, as well as stabilizing crucial reaction intermediates.[96,117,119] For instance, Yin *et al.* demonstrated substantial improvements in CO_2 adsorption and activation capabilities by constructing a Cu/CeO_2 interface compared with commercial Cu without the M/O interfaces. Through precise adjustment of the Cu content, the team also effectively controlled the ratio of low-frequency binding of $*CO_{LFB}$ to high-frequency binding of $*CO_{HFB}$ at the M/O interface. This manipulation resulted in distinct reaction pathways for C_1 and C_{2+} products (Fig. 9(c)).[119]

Silica is an exceptionally stable oxide capable of effectively adsorbing and capturing CO_2.[120] In addition, it exhibits a strong affinity with copper. Its unique catalytic interface with copper has achieved significant success in thermocatalytic hydrogenation reactions.[121,122] Therefore, the modification of copper with silica to construct an active M/O interface offers a novel approach to the design of catalysts for CO_2RR. Zhao *et al.* utilized inorganic SiO_2 aerosols as hydrophobic additives to modulate the catalytic environment of Cu_2O cubes for CO_2RR.[123] The results indicate that compared with Cu_2O, Cu_2O/SiO_2 enhances the selectivity of multi-carbon products (faradaic efficiency for C_{2+} increases from 52.4% to 75.6%) and suppresses hydrogen generation (faradaic efficiency for H_2 decreases from 30.0% to 9.6%). Through a combination of *in situ* spectroscopic analysis, electrocatalytic experiments, and molecular dynamics (MD) simulations, the team comparatively studied the interactions between Cu_2O/SiO_2 catalysts and reaction intermediates, revealing that the weakened buffering effect, enhanced mass transport of CO_2, increased CO_2 capture by SiO_2 aerosols are the primary factors contributing to the improved catalytic performance (Fig. 9(d)). Using DFT calculations, Sinton *et al.* introduced an oxide modulation strategy, wherein silica is incorporated onto the copper surface to create active Cu–SiO_x interface sites.[124] This M/O interface significantly lowers the formation energy of OCOH* and OCCOH*, that is, the crucial intermediates in the ethylene generation pathway. Subsequently, the team synthesized the Cu–SiO_x catalyst using a one-pot co-precipitation method. The results indicated that the MEA electrolyzer based on the Cu–SiO_x catalyst exhibited an impressive 65% ethylene faradaic efficiency at a high partial current density of 215 mA cm^{-2}. Furthermore, the catalyst demonstrated outstanding stability with continuous operation for over 50 hours. The strong metal–support affinity was also harnessed to stabilize electrocatalysts for the CO_2RR. One of our recent works indicated that the deactivation and reconstruction issues of copper-based catalysts under cathodic potentials could be effectively addressed through the construction of an atomic Cu–O–Si interface.[97] *In situ* XAS characterization revealed that the synthesized amorphous $CuSiO_x$ catalyst exhibited exceptionally high electrochemical stability in CO_2RR (Fig. 9(e)). Active Cu species showed no signs of reduction or aggregation,

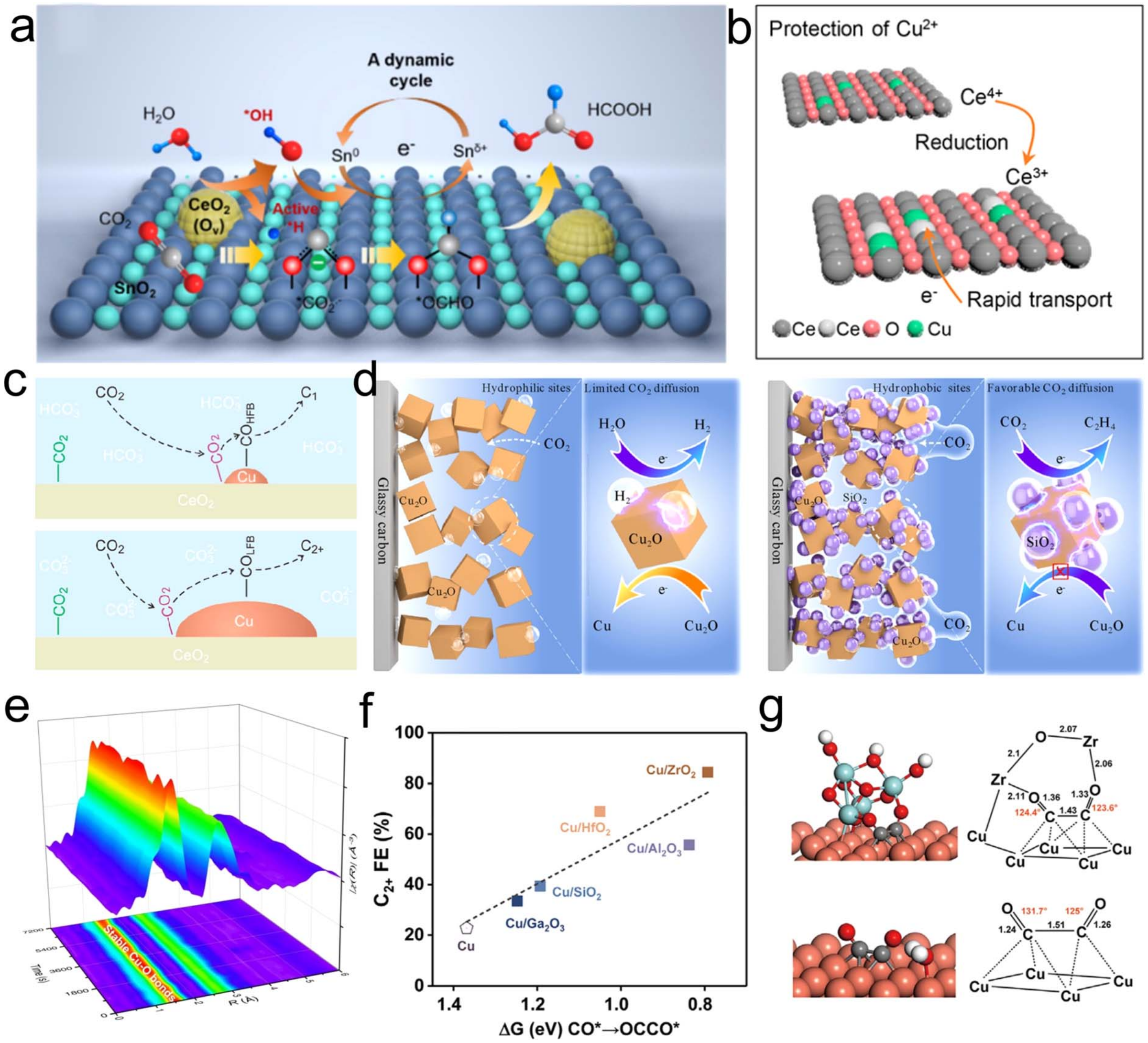

Fig. 9 (a) Proposed reaction mechanism of CO_2 to HCOOH on the Sn–CeO_2 surface. Reproduced with permission from ref. 118. Copyright 2023, American Chemical Society. (b) Scheme of the self-sacrifice mechanism to protect Cu^{2+}. Reproduced with permission from ref. 98. Copyright 2022, American Chemical Society. (c) Proposed CO_2RR mechanism at the Cu and CeO_2 interface. Reproduced with permission from ref. 119. Copyright 2022, American Chemical Society. (d) Schematic depiction of different catalytic microenvironments of Cu_2O and Cu_2O/SiO_2. Reproduced with permission from ref. 123. Copyright 2023, American Chemical Society. (e) *In situ* EXAFS data of $CuSiO_x$ during CO_2RR reaction at −1.4 V *vs.* RHE. Reproduced with permission from ref. 97. Copyright 2023, American Chemical Society. (f) The relationship between Δ*G* of *CO to *OCCO and the Faraday efficiency of C_{2+} products for Cu and Cu/oxide catalysts. (g) The optimized configurations for *OCCO on Cu and Cu-ZrO_2 heterostructure. Reproduced with permission from ref. 22. Copyright 2022, Elsevier.

demonstrating an outstanding resistance against reconstruction that far surpassed that of commercial CuO catalysts. DFT calculations and AIMD simulations further suggested that the interaction with silica enhanced the strength of the Cu–O bonds. Furthermore, Cu–O–Si interface sites were more conducive to the protonation pathway from *CO to *COH, resulting in methane production rather than hydrogen evolution or C–C coupling.

The design of active M/O interface for CO_2RR catalysts has also been extended to other oxides, such as BaO, Al_2O_3, ZrO_2, *etc.*[21,22,125] Sargent *et al.* expanded the modification of Cu catalysts with different alkaline earth metal oxides (Ba, Sr, Ca).[21] They found that BaO significantly improved the faradaic efficiency for C_{2+} alcohols. Mechanistic studies indicated that the increased alcohol selectivity originated from the M/O interface between Cu and alkaline earth metal oxides. The introduction of M/O would favor the formation of C_2 intermediates containing hydroxyl groups (*HCCHOH) rather than hydrocarbon intermediates (*HCC). The study by Wu *et al.* has demonstrated that coupling oxides with Cu to construct Cu/oxide heterogeneous interface could break the constraints of the original scaling relationship between intermediate adsorption on Cu catalysts.[22] This effectively regulated the product distribution in the CO_2RR process (Fig. 9(f)). Specifically, introducing oxides exhibiting strong CO_2*/CO* adsorption on the Cu surface facilitated the activation of CO_2 molecules through Lewis acid–base interactions. Furthermore, the constructed M/O interface could lower the reaction barrier for the C–C coupling step, thereby promoting the generation of multi-carbon products. Notably, the ZrO_2 modified Cu electrode exhibited an 85% selectivity for multi-carbon products (Fig. 9(g)). Generally, the fine construction of a metal/oxide interface holds great promise for enhancing the stability of catalytic active centers, stabilizing crucial reaction intermediates, and optimizing the catalytic microenvironment, which is important for improving the CO_2RR performance.

6. Summary and outlook

Surface/interface engineering has demonstrated its feasibility in developing high-performance electrocatalysts for CO_2RR. In this review, we have summarized the advanced techniques for high-precision characterizations of the catalyst surfaces/interfaces, and systematically discussed the progress in developing various CO_2RR electrocatalysts. As the understanding on atomic-level catalytic structures further deepens, new strategies for customizing catalyst surfaces/interfaces have emerged aiming to optimize the CO_2RR process, such as constructing diatomic-site catalysts for synergistic catalysis, and employing small molecules to precisely manipulate the configurations of surface-adsorbed intermediates. However, surface/interface engineering is facing challenges such as limited manipulation at the atomic scale, insufficient precision in characterization techniques (especially in monitoring the dynamic evolution of surface/interface structures during electrochemical processes to identify real catalytic active sites), and limitations in theoretical models, which calls for more effort to be devoted in this field.

6.1 Atomic-level fine manipulation on the catalyst surfaces/interfaces

As the methodologies in material synthesis and characterization grow more powerful, a major research direction in electrocatalytic CO_2RR is to pursue atomic-level fine manipulation on the catalyst surfaces/interfaces. The most notable example is, arguably, the single-atomic-site catalysts, which feature relatively simple and well-defined structures, and therefore are of great significance for deciphering the complex catalytic processes. However, the CO_2RR process involves the activation of multiple molecular species, and a single active site may not be ideal for activating multiple molecules and mediating the coupling between different intermediates.[14] Therefore, it is desirable to develop more sophisticated synthesis methodologies and to construct multi-atomic-site catalysts, over which CO_2 and H_2O molecules could be synergistically activated and potentially afford complex multi-carbon reduction products. For instance, Chen *et al.* achieved CO_2 activation by constructing Cu_1^0–Cu_1^{x+} interfaces, where Cu_1^{x+} served as a Lewis acid, adsorbing water molecules, while Cu_1^0 acted as a Lewis base, adsorbing CO_2 molecules. This synergistic proton-coupled electron transfer, also known as the "diatomic-activating-bimolecular" mechanism, greatly enhanced CO_2 activation.[14] Liao *et al.* rationally designed a novel MOF with unprecedented heterometallic Sn–Cu dual-site sites. Due to the high oxygen affinity of the SnN_2O_2 site, the Sn–Cu dual sites are more conducive to the asymmetric C–C coupling between *CO and *OCH_2, leading to the predominant production of ethanol.[64] In addition, the atomic-level fine manipulation on catalyst surfaces/interfaces could be extended to other catalytic systems, such as metal catalysts and metal/oxide catalysts. This would surely enrich the library of catalysts available for mediating the CO_2RR process with higher efficiency and controllability.

6.2 High-precision characterization techniques for clarifying the structure–performance relationship

In the CO_2RR process, the catalyst surface/interface, the reaction intermediates, and the microenvironment are all dynamic, and these dynamic components are strongly interacting, which adds to the complexity of the reaction systems and to the difficulty for identifying the structure–performance relationship. In this regard, *in situ* or operando characterization techniques could be of great help. For instance, operando XAS has enabled the probing of the surface/interface status and coordination structures under real operational conditions, which helps to unveil the active role of metal centers during catalysis.[27] Our recent study, employing *in situ* XAS, provides evidence that Cu^{2+} species within CuO exhibit limited electrochemical stability, prone to rapid reduction to Cu^0. Introducing silica to form Cu–O–Si interfaces effectively reinforces the strength of Cu–O bonds, thereby markedly enhancing the stability of Cu^{2+} species.[97] EC-STEM and 4D-STEM have enabled the visualization of surface/interface structures during real reaction processes, and thus directly provide the images of catalyst evolution during CO_2RR.[23] Chen *et al.* provided the first imaging evidence of Cu cluster formation in Cu single-atom catalysts during the CO_2RR process using EC-TEM. This also confirms the finding that small clusters can freely migrate on graphene-like support, attributed to the breaking of C–N and Cu–N bonds.[48] *In situ*/operando infrared spectroscopy and surface-enhanced Raman spectroscopy could monitor the dynamics of reaction intermediates and the microenvironment near the catalytic interface.[31,32] Shao *et al.* employed *in situ* infrared spectroscopy to unveil the mechanism behind the enhanced CO_2 reduction activity on OD-Cu. *In situ* SEIRAS results indicate that the pre-oxidation process can significantly enhance overall CO_2RR activity by (a) enhancing CO_2 activation, (b) increasing CO uptake, and (c) promoting C–C coupling.[126] In the future, these techniques need to go for higher temporal/spatial resolutions so as to pursue superior accuracy and precision. For example, X-ray free-electron laser (XFEL) could be employed as the beam source to conduct XAS and IR measurements, which could afford useful information with higher quality within shorter test times than do synchrotron-radiation beam sources.[2] In addition, the combination of multiple *in situ*/operando techniques could also help to improve the accuracy and efficiency of characterization by simultaneously gathering information from the catalyst surface/interface, the reaction intermediates and the microenvironment. For example, the combination of operando infrared spectroscopy with time-offlight mass spectrometry may offer more precise intermediate information for CO_2RR.[127] Needless to say, such integration of multiple techniques depends on the well-coordinated collaboration between the software and hardware sectors, such as information recording, signal processing, and specifically designed reactors.

6.3 Advanced theoretical modelling and simulation on CO_2RR process at the surface/interface

Thus far, with the aid of theoretical computation, scientists have gained some in-depth understanding on the basic steps of electrochemical CO_2RR process and the reaction pathways, from which some consensuses have be derived. For example, it has been recognized that Cu^0/Cu^+ interface sites could be conducive to C–C coupling, and Cu^{2+} sites would favor *CO binding and further protonation to give methane.[98,106] Despite the remarkable success achieved thus far in theoretical computation, when the local concentrations of relevant species at the catalyst surface and the adsorption/desorption of different intermediates are taken into consideration, the accuracy/precision and the efficiency of theoretical simulation are still far from ideal. Moreover, the catalyst surface/interface generally features a dynamic and non-equilibrated state, rather than the (over)simplified stationary state that is often presumed in computation. Therefore, advanced theoretical models covering multiple time/space scales are needed for simulating the CO_2RR process with higher precision. In this regard, advanced descriptions based on atomistic simulations (such as autonomous workflows and machine learning) could help to tackle these challenges and to establish a clearer image of the electrified interfaces. Autonomous workflows facilitate detailed mechanistic studies by automatically assessing surface states and reaction energies. Machine learning offers opportunities to transform workflows and atomic-level understanding of electrified interfaces, such as generating pertinent geometries for high-throughput computing and autonomous workflows, automating decision-making in workflows (*e.g.*, selecting relevant intermediates and transition states), and replacing costly DFT computations with faster energy evaluations.[128]

Author contributions

C. Z. and C. C. conceived the topic of the review. X. T. and H. Z. wrote the original draft of the manuscript. All authors reviewed and revised the original draft.

Conflicts of interest

There are no conflicts to declare.

Acknowledgements

This work was supported by the National Key R&D Program of China (2023YFB4005100), National Natural Science Foundation of China (21925202, U22B2071, 22302042), Yunnan Provincial Science and Technology Project at Southwest United Graduate School (202302AO370017), International Joint Mission On Climate Change and Carbon Neutrality, Pilot Group Program of the Research Fund for International Senior Scientists (22250710676).

Notes and references

1 O. S. Bushuyev, P. De Luna, C. T. Dinh, L. Tao, G. Saur, J. van de Lagemaat, S. O. Kelley and E. H. Sargent, *Joule*, 2018, **2**, 825–832.
2 L. Li, S. Wang, C. Wan, C. Xu, M. Zuo, Y. Sun and Y. Xie, *Next Energy*, 2023, **1**, 100027.
3 J. Jin, J. Wicks, Q. Min, J. Li, Y. Hu, J. Ma, Y. Wang, Z. Jiang, Y. Xu, R. Lu, G. Si, P. Papangelakis, M. Shakouri, Q. Xiao, P. Ou, X. Wang, Z. Chen, W. Zhang, K. Yu, J. Song, X. Jiang, P. Qiu, Y. Lou, D. Wu, Y. Mao, A. Ozden, C. Wang, B. Y. Xia, X. Hu, V. P. Dravid, Y. M. Yiu, T. K. Sham, Z. Wang, D. Sinton, L. Mai, E. H. Sargent and Y. Pang, *Nature*, 2023, **617**, 724–729.
4 L. Li, X. Li, Y. Sun and Y. Xie, *Chem. Soc. Rev.*, 2022, **51**, 1234–1252.
5 M. Jouny, W. Luc and F. Jiao, *Ind. Eng. Chem. Res.*, 2018, **57**, 2165–2177.
6 X. Tan, Z. Zhuang, Y. Zhang, K. Sun and C. Chen, *Chem. Commun.*, 2023, **59**, 2682–2696.
7 C. J. Chang, Y. A. Lai, Y. C. Chu, C. K. Peng, H. Y. Tan, C. W. Pao, Y. G. Lin, S. F. Hung, H. C. Chen and H. M. Chen, *J. Am. Chem. Soc.*, 2023, **145**, 6953–6965.
8 Y. Zhang, X.-Y. Zhang and W.-Y. Sun, *ACS Catal.*, 2023, **13**, 1545–1553.
9 Y. Jia, H. S. Hsu, W. C. Huang, D. W. Lee, S. W. Lee, T. Y. Chen, L. Zhou, J. H. Wang, K. W. Wang and S. Dai, *Nano Lett.*, 2023, **23**, 2262–2268.
10 Z. Zhang, L. Bian, H. Tian, Y. Liu, Y. Bando, Y. Yamauchi and Z.-L. Wang, *Small*, 2022, **18**, 2107450.
11 A. Vasileff, C. Xu, Y. Jiao, Y. Zheng and S.-Z. Qiao, *Chem*, 2018, **4**, 1809–1831.
12 X. Hu, J. Hu, S. Zheng, Y. Fan, H. Li, S. Zhang, W. Liu, B. Zha, F. Huo and F. Saleem, *Chem.–Asian J.*, 2022, **17**, e202200990.
13 A. Wagner, C. D. Sahm and E. Reisner, *Nat. Catal.*, 2020, **3**, 775–786.
14 J. Jiao, R. Lin, S. Liu, W. C. Cheong, C. Zhang, Z. Chen, Y. Pan, J. Tang, K. Wu, S. F. Hung, H. M. Chen, L. Zheng, Q. Lu, X. Yang, B. Xu, H. Xiao, J. Li, D. Wang, Q. Peng, C. Chen and Y. Li, *Nat. Chem.*, 2019, **11**, 222–228.
15 H. Xu, D. Rebollar, H. He, L. Chong, Y. Liu, C. Liu, C.-J. Sun, T. Li, J. V. Muntean, R. E. Winans, D.-J. Liu and T. Xu, *Nat. Energy*, 2020, **5**, 623–632.
16 J. Gao, A. Bahmanpour, O. Krocher, S. M. Zakeeruddin, D. Ren and M. Gratzel, *Nat. Chem.*, 2023, **15**, 705–713.
17 H. Huang, H. Jia, Z. Liu, P. Gao, J. Zhao, Z. Luo, J. Yang and J. Zeng, *Angew. Chem., Int. Ed.*, 2017, **56**, 3594–3598.
18 Y. Deng, J. Zhao, S. Wang, R. Chen, J. Ding, H. J. Tsai, W. J. Zeng, S. F. Hung, W. Xu, J. Wang, F. Jaouen, X. Li, Y. Huang and B. Liu, *J. Am. Chem. Soc.*, 2023, **145**, 7242–7251.

19 Y. Pan, R. Lin, Y. Chen, S. Liu, W. Zhu, X. Cao, W. Chen, K. Wu, W. C. Cheong, Y. Wang, L. Zheng, J. Luo, Y. Lin, Y. Liu, C. Liu, J. Li, Q. Lu, X. Chen, D. Wang, Q. Peng, C. Chen and Y. Li, *J. Am. Chem. Soc.*, 2018, **140**, 4218–4221.

20 Q. Hao, H.-X. Zhong, J.-Z. Wang, K.-H. Liu, J.-M. Yan, Z.-H. Ren, N. Zhou, X. Zhao, H. Zhang, D.-X. Liu, X. Liu, L.-W. Chen, J. Luo and X.-B. Zhang, *Nat. Synth.*, 2022, **1**, 719–728.

21 A. Xu, S.-F. Hung, A. Cao, Z. Wang, N. Karmodak, J. E. Huang, Y. Yan, A. Sedighian Rasouli, A. Ozden, F.-Y. Wu, Z.-Y. Lin, H.-J. Tsai, T.-J. Lee, F. Li, M. Luo, Y. Wang, X. Wang, J. Abed, Z. Wang, D.-H. Nam, Y. C. Li, A. H. Ip, D. Sinton, C. Dong and E. H. Sargent, *Nat. Catal.*, 2022, **5**, 1081–1088.

22 X. Li, Q. Liu, J. Wang, D. Meng, Y. Shu, X. Lv, B. Zhao, H. Yang, T. Cheng, Q. Gao, L. Li and H. B. Wu, *Chem*, 2022, **8**, 2148–2162.

23 Y. Yang, S. Louisia, S. Yu, J. Jin, I. Roh, C. Chen, M. V. Fonseca Guzman, J. Feijóo, P.-C. Chen, H. Wang, C. J. Pollock, X. Huang, Y.-T. Shao, C. Wang, D. A. Muller, H. D. Abruña and P. Yang, *Nature*, 2023, **614**, 262–269.

24 S. G. Han, D. D. Ma and Q. L. Zhu, *Small Methods*, 2021, **5**, e2100102.

25 C. Liu, Y. Wu, K. Sun, J. Fang, A. Huang, Y. Pan, W.-C. Cheong, Z. Zhuang, Z. Zhuang, Q. Yuan, H. L. Xin, C. Zhang, J. Zhang, H. Xiao, C. Chen and Y. Li, *Chem*, 2021, **7**, 1297–1307.

26 Z. Chen, A. Huang, K. Yu, T. Cui, Z. Zhuang, S. Liu, J. Li, R. Tu, K. Sun, X. Tan, J. Zhang, D. Liu, Y. Zhang, P. Jiang, Y. Pan, C. Chen, Q. Peng and Y. Li, *Energy Environ. Sci.*, 2021, **14**, 3430–3437.

27 J. Wang, C.-S. Hsu, T.-S. Wu, T.-S. Chan, N.-T. Suen, J.-F. Lee and H. M. Chen, *Nat. Commun.*, 2023, **14**, 6576.

28 J. Timoshenko, A. Bergmann, C. Rettenmaier, A. Herzog, R. M. Arán-Ais, H. S. Jeon, F. T. Haase, U. Hejral, P. Grosse, S. Kühl, E. M. Davis, J. Tian, O. Magnussen and B. Roldan Cuenya, *Nat. Catal.*, 2022, **5**, 259–267.

29 H. T. Chung, D. A. Cullen, D. Higgins, B. T. Sneed, E. F. Holby, K. L. More and P. Zelenay, *Science*, 2017, **357**, 479–484.

30 C. Chen, Y. Li, A. Huang, X. Liu, J. Li, Y. Zhang, Z. Chen, Z. Zhuang, Y. Wu, W.-C. Cheong, X. Tan, K. Sun, Z. Xu, D. Liu, Z. Wang, K. Zhou and C. Chen, *J. Am. Chem. Soc.*, 2023, **145**, 21273–21283.

31 S. Zhu, T. Li, W.-B. Cai and M. Shao, *ACS Energy Lett.*, 2019, **4**, 682–689.

32 C. Long, X. Liu, K. Wan, Y. Jiang, P. An, C. Yang, G. Wu, W. Wang, J. Guo, L. Li, K. Peng, Q. Li, C. Cui, S. Liu, T. Tan and Z. Tang, *Sci. Adv.*, 2023, **9**, eadi6119.

33 J. Zhang, P. Yu, C. Peng, X. Lv, Z. Liu, T. Cheng and G. Zheng, *ACS Catal.*, 2023, **13**, 7170–7177.

34 A. Dutta, I. Zelocualtecatl Montiel, K. Kiran, A. Rieder, V. Grozovski, L. Gut and P. Broekmann, *ACS Catal.*, 2021, **11**, 4988–5003.

35 I. Zelocualtecatl Montiel, A. Dutta, K. Kiran, A. Rieder, A. Iarchuk, S. Vesztergom, M. Mirolo, I. Martens, J. Drnec and P. Broekmann, *ACS Catal.*, 2022, **12**, 10872–10886.

36 F. Li, X. V. Medvedeva, J. J. Medvedev, E. Khairullina, H. Engelhardt, S. Chandrasekar, Y. Guo, J. Jin, A. Lee, H. Thérien-Aubin, A. Ahmed, Y. Pang and A. Klinkova, *Nat. Catal.*, 2021, **4**, 479–487.

37 R. Amirbeigiarab, J. Tian, A. Herzog, C. Qiu, A. Bergmann, B. Roldan Cuenya and O. M. Magnussen, *Nat. Catal.*, 2023, **6**, 837–846.

38 M. Munz, J. Poon, W. Frandsen, B. R. Cuenya and C. S. Kley, *J. Am. Chem. Soc.*, 2023, **145**, 5242–5251.

39 D. Zhao, K. Yu, P. Song, W. Feng, B. Hu, W.-C. Cheong, Z. Zhuang, S. Liu, K. Sun, J. Zhang and C. Chen, *Energy Environ. Sci.*, 2022, **15**, 3795–3804.

40 L. Han, S. Song, M. Liu, S. Yao, Z. Liang, H. Cheng, Z. Ren, W. Liu, R. Lin, G. Qi, X. Liu, Q. Wu, J. Luo and H. L. Xin, *J. Am. Chem. Soc.*, 2020, **142**, 12563–12567.

41 J. Gu, C. S. Hsu, L. Bai, H. Chen and X. Hu, *Science*, 2019, **364**, 1091–1094.

42 K. Zuraiqi, A. Zavabeti, J. Clarke-Hannaford, B. J. Murdoch, K. Shah, M. J. S. Spencer, C. F. McConville, T. Daeneke and K. Chiang, *Energy Environ. Sci.*, 2022, **15**, 595–600.

43 Z. Zhang, J. Zhu, S. Chen, W. Sun and D. Wang, *Angew. Chem., Int. Ed.*, 2023, **62**, e202215136.

44 Y. Wu, Z. Jiang, X. Lu, Y. Liang and H. Wang, *Nature*, 2019, **575**, 639–642.

45 C. Chen, J. Li, X. Tan, Y. Zhang, Y. Li, C. He, Z. Xu, C. Zhang and C. Chen, *EES Catal.*, 2024, **2**, 71–93.

46 J. R. Huang, X. F. Qiu, Z. H. Zhao, H. L. Zhu, Y. C. Liu, W. Shi, P. Q. Liao and X. M. Chen, *Angew. Chem., Int. Ed.*, 2022, **61**, e202210985.

47 L. Liu and A. Corma, *Trends Chem.*, 2020, **2**, 383–400.

48 C.-S. Hsu, J. Wang, Y.-C. Chu, J.-H. Chen, C.-Y. Chien, K.-H. Lin, L. D. Tsai, H.-C. Chen, Y.-F. Liao, N. Hiraoka, Y.-C. Cheng and H. M. Chen, *Nat. Commun.*, 2023, **14**, 5245.

49 C. Jia, S. Li, Y. Zhao, R. K. Hocking, W. Ren, X. Chen, Z. Su, W. Yang, Y. Wang, S. Zheng, F. Pan and C. Zhao, *Adv. Funct. Mater.*, 2021, **31**, 2107072.

50 D. Karapinar, N. T. Huan, N. Ranjbar Sahraie, J. Li, D. Wakerley, N. Touati, S. Zanna, D. Taverna, L. H. Galvao Tizei, A. Zitolo, F. Jaouen, V. Mougel and M. Fontecave, *Angew. Chem., Int. Ed.*, 2019, **58**, 15098–15103.

51 L. Zhang, X. Yang, Q. Yuan, Z. Wei, J. Ding, T. Chu, C. Rong, Q. Zhang, Z. Ye, F.-Z. Xuan, Y. Zhai, B. Zhang and X. Yang, *Nat. Commun.*, 2023, **14**, 8311.

52 X. Sun, Y. Tuo, C. Ye, C. Chen, Q. Lu, G. Li, P. Jiang, S. Chen, P. Zhu, M. Ma, J. Zhang, J. H. Bitter, D. Wang and Y. Li, *Angew. Chem., Int. Ed.*, 2021, **60**, 23614–23618.

53 M. Wang, Y. Yao, Y. Tian, Y. Yuan, L. Wang, F. Yang, J. Ren, X. Hu, F. Wu, S. Zhang, J. Wu and J. Lu, *Adv. Mater.*, 2023, **35**, e2210658.

54 Y. Y. Birdja, E. Pérez-Gallent, M. C. Figueiredo, A. J. Göttle, F. Calle-Vallejo and M. T. M. Koper, *Nat. Energy*, 2019, **4**, 732–745.

55 K. Sun, K. Yu, J. Fang, Z. Zhuang, X. Tan, Y. Wu, L. Zeng, Z. Zhuang, Y. Pan and C. Chen, *Adv. Mater.*, 2022, **34**, e2206478.

56 Q. Qu, S. Ji, Y. Chen, D. Wang and Y. Li, *Chem. Sci.*, 2021, **12**, 4201–4215.

57 Z. Zhang, S. Chen, J. Zhu, C. Ye, Y. Mao, B. Wang, G. Zhou, L. Mai, Z. Wang, X. Liu and D. Wang, *Nano Lett.*, 2023, **23**, 2312–2320.
58 L. Jiao, J. Zhu, Y. Zhang, W. Yang, S. Zhou, A. Li, C. Xie, X. Zheng, W. Zhou, S. H. Yu and H. L. Jiang, *J. Am. Chem. Soc.*, 2021, **143**, 19417–19424.
59 W. Zhu, L. Zhang, S. Liu, A. Li, X. Yuan, C. Hu, G. Zhang, W. Deng, K. Zang, J. Luo, Y. Zhu, M. Gu, Z. J. Zhao and J. Gong, *Angew. Chem., Int. Ed.*, 2020, **59**, 12664–12668.
60 W. Ren, X. Tan, W. Yang, C. Jia, S. Xu, K. Wang, S. C. Smith and C. Zhao, *Angew. Chem., Int. Ed.*, 2019, **58**, 6972–6976.
61 J. D. Yi, X. Gao, H. Zhou, W. Chen and Y. Wu, *Angew. Chem., Int. Ed.*, 2022, **61**, e202212329.
62 S. Li, A. Guan, C. Yang, C. Peng, X. Lv, Y. Ji, Y. Quan, Q. Wang, L. Zhang and G. Zheng, *ACS Mater. Lett.*, 2021, **3**, 1729–1737.
63 K. Yang, Y. Sun, S. Chen, M. Li, M. Zheng, L. Ma, W. Fan, Y. Zheng, Q. Li and J. Duan, *Small*, 2023, **19**, 2301536.
64 Z.-H. Zhao, J.-R. Huang, P.-Q. Liao and X.-M. Chen, *J. Am. Chem. Soc.*, 2023, **145**, 26783–26790.
65 R. Wang, J. Liu, Q. Huang, L. Z. Dong, S. L. Li and Y. Q. Lan, *Angew. Chem., Int. Ed.*, 2021, **60**, 19829–19835.
66 S. Jeong, M.-H. Choi, G. S. Jagdale, Y. Zhong, N. P. Siepser, Y. Wang, X. Zhan, L. A. Baker and X. Ye, *J. Am. Chem. Soc.*, 2022, **144**, 12673–12680.
67 S. Liu, H. Tao, L. Zeng, Q. Liu, Z. Xu, Q. Liu and J.-L. Luo, *J. Am. Chem. Soc.*, 2017, **139**, 2160–2163.
68 B. Ren, G. Wen, R. Gao, D. Luo, Z. Zhang, W. Qiu, Q. Ma, X. Wang, Y. Cui, L. Ricardez-Sandoval, A. Yu and Z. Chen, *Nat. Commun.*, 2022, **13**, 2486.
69 Z. Wu, H. Wu, W. Cai, Z. Wen, B. Jia, L. Wang, W. Jin and T. Ma, *Angew. Chem., Int. Ed.*, 2021, **60**, 12554–12559.
70 L. Lu, X. Sun, J. Ma, D. Yang, H. Wu, B. Zhang, J. Zhang and B. Han, *Angew. Chem., Int. Ed.*, 2018, **57**, 14149–14153.
71 X. Li, X. Wu, X. Lv, J. Wang and H. B. Wu, *Chem Catal.*, 2022, **2**, 262–291.
72 F. Li, A. Thevenon, A. Rosas-Hernandez, Z. Wang, Y. Li, C. M. Gabardo, A. Ozden, C. T. Dinh, J. Li, Y. Wang, J. P. Edwards, Y. Xu, C. McCallum, L. Tao, Z. Q. Liang, M. Luo, X. Wang, H. Li, C. P. O'Brien, C. S. Tan, D. H. Nam, R. Quintero-Bermudez, T. T. Zhuang, Y. C. Li, Z. Han, R. D. Britt, D. Sinton, T. Agapie, J. C. Peters and E. H. Sargent, *Nature*, 2020, **577**, 509–513.
73 A. K. Buckley, M. Lee, T. Cheng, R. V. Kazantsev, D. M. Larson, W. A. Goddard III, F. D. Toste and F. M. Toma, *J. Am. Chem. Soc.*, 2019, **141**, 7355–7364.
74 D. M. Koshy, S. A. Akhade, A. Shugar, K. Abiose, J. Shi, S. Liang, J. S. Oakdale, S. E. Weitzner, J. B. Varley, E. B. Duoss, S. E. Baker, C. Hahn, Z. Bao and T. F. Jaramillo, *J. Am. Chem. Soc.*, 2021, **143**, 14712–14725.
75 A. K. Buckley, T. Cheng, M. H. Oh, G. M. Su, J. Garrison, S. W. Utan, C. Zhu, F. D. Toste, W. A. Goddard and F. M. Toma, *ACS Catal.*, 2021, **11**, 9034–9042.
76 M. Fan, R. K. Miao, P. Ou, Y. Xu, Z. Y. Lin, T. J. Lee, S. F. Hung, K. Xie, J. E. Huang, W. Ni, J. Li, Y. Zhao, A. Ozden, C. P. O'Brien, Y. Chen, Y. C. Xiao, S. Liu, J. Wicks, X. Wang, J. Abed, E. Shirzadi, E. H. Sargent and D. Sinton, *Nat. Commun.*, 2023, **14**, 3314.
77 K. P. Kuhl, E. R. Cave, D. N. Abram and T. F. Jaramillo, *Energy Environ. Sci.*, 2012, **5**, 7050–7059.
78 C. G. Morales-Guio, E. R. Cave, S. A. Nitopi, J. T. Feaster, L. Wang, K. P. Kuhl, A. Jackson, N. C. Johnson, D. N. Abram, T. Hatsukade, C. Hahn and T. F. Jaramillo, *Nat. Catal.*, 2018, **1**, 764–771.
79 C. Zhu, L. Zhou, Z. Zhang, C. Yang, G. Shi, S. Zhao, H. Gu, J. Wu, X. Gao, Y. Li, K. Liu, S. Dai and L. Zhang, *Chem*, 2022, **8**, 3288–3301.
80 J. Huang, M. Mensi, E. Oveisi, V. Mantella and R. Buonsanti, *J. Am. Chem. Soc.*, 2019, **141**, 2490–2499.
81 Y. Ma, J. Yu, M. Sun, B. Chen, X. Zhou, C. Ye, Z. Guan, W. Guo, G. Wang, S. Lu, D. Xia, Y. Wang, Z. He, L. Zheng, Q. Yun, L. Wang, J. Zhou, P. Lu, J. Yin, Y. Zhao, Z. Luo, L. Zhai, L. Liao, Z. Zhu, R. Ye, Y. Chen, Y. Lu, S. Xi, B. Huang, C. S. Lee and Z. Fan, *Adv. Mater.*, 2022, **34**, 2110607.
82 P. C. Chen, C. Chen, Y. Yang, A. L. Maulana, J. Jin, J. Feijoo and P. Yang, *J. Am. Chem. Soc.*, 2023, **145**, 10116–10125.
83 X. Zhou, A. Zhang, B. Chen, S. Zhu, Y. Cui, L. Bai, J. Yu, Y. Ge, Q. Yun, L. Li, B. Huang, L. Liao, J. Fu, Q. Wa, G. Wang, Z. Huang, L. Zheng, Y. Ren, S. Li, G. Liu, L. Zhai, Z. Li, J. Liu, Y. Chen, L. Ma, C. Ling, J. Wang, Z. Fan, Y. Du, M. Shao and H. Zhang, *Adv. Mater.*, 2023, **35**, 2304414.
84 J. Zhao, P. Zhang, T. Yuan, D. Cheng, S. Zhen, H. Gao, T. Wang, Z. J. Zhao and J. Gong, *J. Am. Chem. Soc.*, 2023, **145**, 6622–6627.
85 K. Qi, Y. Zhang, N. Onofrio, E. Petit, X. Cui, J. Ma, J. Fan, H. Wu, W. Wang, J. Li, J. Liu, Y. Zhang, Y. Wang, G. Jia, J. Wu, L. Lajaunie, C. Salameh and D. Voiry, *Nat. Catal.*, 2023, **6**, 319–331.
86 P. Li, J. Bi, J. Liu, Y. Wang, X. Kang, X. Sun, J. Zhang, Z. Liu, Q. Zhu and B. Han, *J. Am. Chem. Soc.*, 2023, **145**, 4675–4682.
87 V. Okatenko, A. Loiudice, M. A. Newton, D. C. Stoian, A. Blokhina, A. N. Chen, K. Rossi and R. Buonsanti, *J. Am. Chem. Soc.*, 2023, **145**, 5370–5383.
88 Y. Wang, L. Cao, N. J. Libretto, X. Li, C. Li, Y. Wan, C. He, J. Lee, J. Gregg, H. Zong, D. Su, J. T. Miller, T. Mueller and C. Wang, *J. Am. Chem. Soc.*, 2019, **141**, 16635–16642.
89 M. Chhetri, M. Wan, Z. Jin, J. Yeager, C. Sandor, C. Rapp, H. Wang, S. Lee, C. J. Bodenschatz, M. J. Zachman, F. Che and M. Yang, *Nat. Commun.*, 2023, **14**, 3075.
90 Y. Cao, S. Chen, S. Bo, W. Fan, J. Li, C. Jia, Z. Zhou, Q. Liu, L. Zheng and F. Zhang, *Angew. Chem., Int. Ed.*, 2023, **62**, e202303048.
91 T. Zheng, C. Liu, C. Guo, M. Zhang, X. Li, Q. Jiang, W. Xue, H. Li, A. Li, C. W. Pao, J. Xiao, C. Xia and J. Zeng, *Nat. Nanotechnol.*, 2021, **16**, 1386–1393.
92 Y. Zhou, F. Che, M. Liu, C. Zou, Z. Liang, P. De Luna, H. Yuan, J. Li, Z. Wang, H. Xie, H. Li, P. Chen, E. Bladt, R. Quintero-Bermudez, T. K. Sham, S. Bals, J. Hofkens, D. Sinton, G. Chen and E. H. Sargent, *Nat. Chem.*, 2018, **10**, 974–980.

93 W. Ma, S. Xie, T. Liu, Q. Fan, J. Ye, F. Sun, Z. Jiang, Q. Zhang, J. Cheng and Y. Wang, *Nat. Catal.*, 2020, **3**, 478–487.

94 T. Wang, J. Chen, X. Ren, J. Zhang, J. Ding, Y. Liu, K. H. Lim, J. Wang, X. Li, H. Yang, Y. Huang, S. Kawi and B. Liu, *Angew. Chem., Int. Ed.*, 2023, **62**, e202211174.

95 L. Lv, R. Lu, J. Zhu, R. Yu, W. Zhang, E. Cui, X. Chen, Y. Dai, L. Cui, J. Li, L. Zhou, W. Chen, Z. Wang and L. Mai, *Angew. Chem., Int. Ed.*, 2023, **62**, e202303117.

96 Y. X. Duan, Y. T. Zhou, Z. Yu, D. X. Liu, Z. Wen, J. M. Yan and Q. Jiang, *Angew. Chem., Int. Ed.*, 2021, **60**, 8798–8802.

97 X. Tan, K. Sun, Z. Zhuang, B. Hu, Y. Zhang, Q. Liu, C. He, Z. Xu, C. Chen, H. Xiao and C. Chen, *J. Am. Chem. Soc.*, 2023, **145**, 8656–8664.

98 X. Zhou, J. Shan, L. Chen, B. Y. Xia, T. Ling, J. Duan, Y. Jiao, Y. Zheng and S. Z. Qiao, *J. Am. Chem. Soc.*, 2022, **144**, 2079–2084.

99 T.-C. Chou, C.-C. Chang, H.-L. Yu, W.-Y. Yu, C.-L. Dong, J.-J. Velasco-Vélez, C.-H. Chuang, L.-C. Chen, J.-F. Lee, J.-M. Chen and H.-L. Wu, *J. Am. Chem. Soc.*, 2020, **142**, 2857–2867.

100 S. Gao, Y. Lin, X. Jiao, Y. Sun, Q. Luo, W. Zhang, D. Li, J. Yang and Y. Xie, *Nature*, 2016, **529**, 68–71.

101 C. W. Li, J. Ciston and M. W. Kanan, *Nature*, 2014, **508**, 504–507.

102 C. W. Li and M. W. Kanan, *J. Am. Chem. Soc.*, 2012, **134**, 7231–7234.

103 X. Y. Zhang, Z. X. Lou, J. Chen, Y. Liu, X. Wu, J. Y. Zhao, H. Y. Yuan, M. Zhu, S. Dai, H. F. Wang, C. Sun, P. F. Liu and H. G. Yang, *Nat. Commun.*, 2023, **14**, 7681.

104 Y. Chen, C. W. Li and M. W. Kanan, *J. Am. Chem. Soc.*, 2012, **134**, 19969–19972.

105 Y. Chen and M. W. Kanan, *J. Am. Chem. Soc.*, 2012, **134**, 1986–1989.

106 X. Yuan, S. Chen, D. Cheng, L. Li, W. Zhu, D. Zhong, Z. J. Zhao, J. Li, T. Wang and J. Gong, *Angew. Chem., Int. Ed.*, 2021, **60**, 15344–15347.

107 X. Wang, Y. Jiang, K. Mao, W. Gong, D. Duan, J. Ma, Y. Zhong, J. Li, H. Liu, R. Long and Y. Xiong, *J. Am. Chem. Soc.*, 2022, **144**, 22759–22766.

108 C. Chen, S. Yu, Y. Yang, S. Louisia, I. Roh, J. Jin, S. Chen, P.-C. Chen, Y. Shan and P. Yang, *Nat. Catal.*, 2022, **5**, 878–887.

109 P. Wang, H. Yang, C. Tang, Y. Wu, Y. Zheng, T. Cheng, K. Davey, X. Huang and S. Z. Qiao, *Nat. Commun.*, 2022, **13**, 3754.

110 K. Yao, J. Li, H. Wang, R. Lu, X. Yang, M. Luo, N. Wang, Z. Wang, C. Liu, T. Jing, S. Chen, E. Cortés, S. A. Maier, S. Zhang, T. Li, Y. Yu, Y. Liu, X. Kang and H. Liang, *J. Am. Chem. Soc.*, 2022, **144**, 14005–14011.

111 J. S. Woertink, P. J. Smeets, M. H. Groothaert, M. A. Vance, B. F. Sels, R. A. Schoonheydt and E. I. Solomon, *Proc. Natl. Acad. Sci. U. S. A.*, 2009, **106**, 18908–18913.

112 S. Xu, S. Chansai, C. Stere, B. Inceesungvorn, A. Goguet, K. Wangkawong, S. F. R. Taylor, N. Al-Janabi, C. Hardacre, P. A. Martin and X. Fan, *Nat. Catal.*, 2019, **2**, 142–148.

113 D. Yao, C. Tang, A. Vasileff, X. Zhi, Y. Jiao and S. Z. Qiao, *Angew. Chem., Int. Ed.*, 2021, **60**, 18178–18184.

114 L. Lin, X. He, X. G. Zhang, W. Ma, B. Zhang, D. Wei, S. Xie, Q. Zhang, X. Yi and Y. Wang, *Angew. Chem., Int. Ed.*, 2023, **62**, e202214959.

115 H. Zhao, R. Yu, S. Ma, K. Xu, Y. Chen, K. Jiang, Y. Fang, C. Zhu, X. Liu, Y. Tang, L. Wu, Y. Wu, Q. Jiang, P. He, Z. Liu and L. Tan, *Nat. Catal.*, 2022, **5**, 818–831.

116 C. Xie, C. Chen, Y. Yu, J. Su, Y. Li, G. A. Somorjai and P. Yang, *Nano Lett.*, 2017, **17**, 3798–3802.

117 D. Gao, Y. Zhang, Z. Zhou, F. Cai, X. Zhao, W. Huang, Y. Li, J. Zhu, P. Liu, F. Yang, G. Wang and X. Bao, *J. Am. Chem. Soc.*, 2017, **139**, 5652–5655.

118 H. Liu, B. Li, Z. Liu, Z. Liang, H. Chuai, H. Wang, S. N. Lou, Y. Su, S. Zhang and X. Ma, *ACS Catal.*, 2023, **13**, 5033–5042.

119 J. Yin, Z. Gao, F. Wei, C. Liu, J. Gong, J. Li, W. Li, L. Xiao, G. Wang, J. Lu and L. Zhuang, *ACS Catal.*, 2022, **12**, 1004–1011.

120 P. Goyal, M. J. Purdue and S. Farooq, *Ind. Eng. Chem. Res.*, 2019, **58**, 19611–19622.

121 C. Xu, G. Chen, Y. Zhao, P. Liu, X. Duan, L. Gu, G. Fu, Y. Yuan and N. Zheng, *Nat. Commun.*, 2018, **9**, 3367.

122 J. Sun, J. Yu, Q. Ma, F. Meng, X. Wei, Y. Sun and N. Tsubaki, *Sci. Adv.*, 2018, **4**, 3275.

123 T. Zhao, J. Li, J. Liu, F. Liu, K. Xu, M. Yu, W. Xu and F. Cheng, *ACS Catal.*, 2023, **13**, 4444–4453.

124 J. Li, A. Ozden, M. Wan, Y. Hu, F. Li, Y. Wang, R. R. Zamani, D. Ren, Z. Wang, Y. Xu, D.-H. Nam, J. Wicks, B. Chen, X. Wang, M. Luo, M. Graetzel, F. Che, E. H. Sargent and D. Sinton, *Nat. Commun.*, 2021, **12**, 2808.

125 S. Chen, B. Wang, J. Zhu, L. Wang, H. Ou, Z. Zhang, X. Liang, L. Zheng, L. Zhou, Y. Q. Su, D. Wang and Y. Li, *Nano Lett.*, 2021, **21**, 7325–7331.

126 E. P. Delmo, Y. Wang, Y. Song, S. Zhu, H. Zhang, H. Xu, T. Li, J. Jang, Y. Kwon, Y. Wang and M. Shao, *J. Am. Chem. Soc.*, 2024, **146**, 1935–1945.

127 H. Ren, M. Kovalev, Z. Weng, M. Z. Muhamad, H. Ma, Y. Sheng, L. Sun, J. Wang, S. Rihm, W. Yang, A. A. Lapkin and J. W. Ager, *Nat. Catal.*, 2022, **5**, 1169–1179.

128 S. N. Steinmann and Z. W. Seh, *Nat. Rev. Mater.*, 2021, **6**, 289–291.